The CASTOR Mission

Patrick Côté[1,*], Tyrone E. Woods[2], John B. Hutchings[1], Jason D. Rhodes[3], Rubén Sánchez-Janssen[4], Alan D. Scott[5], John Pazder[1], Melissa Amenouche[1], Michael Balogh[6,7], Simon Blouin[8], Alain Cournoyer[9], Maria R. Drout[10], Nick Kuzmin[11], Katherine J. Mack[12], Laura Ferrarese[1], Wesley C. Fraser[1], Sarah C. Gallagher[13], Frédéric Grandmont[9], Daryl Haggard[14], Paul Harrison[15], Vincent Hénault-Brunet[16], JJ Kavelaars[1], Viraja Khatu[17], Joel C. Roediger[18], Jason Rowe[19], Marcin Sawicki[16], Jesper Skottfelt[20], Matt Taylor[11], Ludo van Waerbeke[21], Laurie Amen[14], Dhananjhay Bansal[1], Martin Bergeron[18], Toby Brown[1], Greg Burley[1], Hum Chand[22], Isaac Cheng[6,23], Ryan Cloutier[24], Nolan Dickson[16], Oleg Djazovski[18], Ivana Damjanov[16], James Doherty[18], Kyle Finner[25], Macarena García Del Valle Espinosa[26], Jennifer Glover[14], Ana I. Gómez de Castro[27], Or Graur[28], Tim Hardy[1], Michelle Kao[6], Denis Leahy[11], Deborah Lokhorst[1], Alex I. Malz[29], Allison Man[21], Madeline A. Marshall[1,30], Sean McGee[31], Ryan McKenzie[15], Kai Michaud[1], Surhud S More[32], David Morris[33], Patrick W. Morris[25], Thibaud Moutard[34], Wasi Naqvi[35], Matt Nicholl[36], Gaël Noirot[16,43], M. S Oey[37], Cyrielle Opitom[26], Samir Salim[38], Bryan R. Scott[39], Charles A. Shapiro[3], Daniel Stern[3], Annapurni Subramaniam[40], David Thilke[41], Ivan Wevers[1], Dmitri Vorobiev[42], L. Y. Aaron Yung[43], Frédéric Zamkotsian[34], Suzanne Aigrain[44], Anahita Alavi[25], Martin Barstow[45], Peter Bartosik[5], Hadleigh Bluhm[11], Jo Bovy[10], Peter Cameron[5], R. G. Carlberg[10], Jessie L. Christiansen[25], Yuyang Chen[10], Paul Crowther[46], Kristen Dage[47], Aaron L. Dotter[48], Patrick Dufour[49], Jean Dupuis[18], Ben Dryer[20], Angaraj Duara[20], Gwendolyn M. Eadie[50], Marielle R. Eduardo[8], Vincente Estrada-Carpenter[16], Sébastien Fabbro[1], Andreas Faisst[25], Nicole M. Ford[14], Morgan Fraser[51], Boris T. Gaensicke[52], Shashkiran Ganesh[53], Poshak Gandhi[54], Melissa L. Graham[55], Rebecca Hamel[16], Martin Hellmich[16], John Hennessy[3], Kaitlyn Hessel[8,24], Jeremy Heyl[21], Catherine Heymans[26], Yashar Hezaveh[49], Renee Hlozek[10], Michael E. Hoenk[3], Andrew Holland[20], Eric Huff[3], Ian Hutchinson[45], Ikuru Iwata[16,56], April D. Jewell[3], Doug Johnstone[1], Maia Jones[4], Todd Jones[3], Dustin Lang[12], Jon Lapington[45], Justin Larivière[9], Cameron Lawlor-Forsyth[6,7], Denis Laurin[18], Charles Lee[2], Ronan Legin[49], Ting S. Li[10], Sungsoon Lim[57], Bethany Ludwig[10], Matt Kozun[5], Vivek. M[40], Robert Mann[26], Alan W. McConnachie[1], Evan McDonough[58], Stanimir Metchev[13], David R. Miller[21], Takashi Moriya[56], Cameron Morgan[6,7], Julio Navarro[8], Yaël Nazé[59], Shouleh Nikzad[3], Vivek Oad[11], Nathalie Ouellette[49], Emily K. Pass[60], Will J. Percival[6], Laurence Perreault Levasseur[49], Joe Postma[11], Nayyer Raza[14], Gordon T. Richards[61], Harvey Richer[21], Carmelle Robert[62], Erik Rosolowsky[63], John J. Ruan[19], Sarah Rugheimer[64], Samar Safi-Harb[2], Kanak Saha[32], Vicky Scowcroft[65], Federico Sestito[8], Himanshu Sharma[22], James Sikora[19], Gregory R. Sivakoff[63], Thirupathi Sivarani[40], Patrick Smith[4], Warren Soh[5], Robert Sorba[16], Smitha Subramanian[40], Hossen Teimoorinia[1], Harry I. Teplitz[25], Shaylin Thadani[66], Shavon Thadani[66], Aaron Tohuvavohu[10], Kim A. Venn[8], Nicholas Vieira[14], Jeremy J. Webb[67], Paul Wiegert[13], Ryan Wierckx[2], Yanqin Wu[10], Jade Yeung[2], Sukyoung K. Yi[68]

[1]National Research Council of Canada, Herzberg Astronomy & Astrophysics Research Centre, Victoria, BC, V9E 2E7, Canada

[2]Department of Physics and Astronomy, University of Manitoba, Winnipeg, Manitoba R3T 2N2, Canada

[3]Jet Propulsion Laboratory, California Institute of Technology, 4800 Oak Grove Drive, Pasadena, CA 91109, USA

[4]UK Astronomy Technology Centre, Royal Observatory, Blackford Hill, Edinburgh EH9 3HJ, UK

[5]Honeywell Aerospace, 155 Sheldon Drive, Cambridge, ON N1R 7H6, Canada

[6]Department of Physics and Astronomy, University of Waterloo, Waterloo, ON N2L 3G1, Canada

[7]Waterloo Centre for Astrophysics, University of Waterloo, Waterloo, ON N2L 3G1 Canada

[8]Department of Physics and Astronomy, University of Victoria, PO Box 3055, STN CSC, Victoria BC V8W 3P6, Canada

[9]ABB Inc., Measurement and Analytics Division, 3400 Rue Pierre-Ardouin, Québec, QC G1P 0B2, Canada

[10]David A. Dunlap Department of Astronomy & Astrophysics, University of Toronto, 50 St. George Street, Toronto, ON M5S 3H4, Canada

[11]Department of Physics and Astronomy, University of Calgary, Calgary, AB T2N 1N4, Canada

[12]Perimeter Institute of Theoretical Physics, 31 Caroline St. N., Waterloo, ON, N2L 2Y5, Canada

[13]Department of Physics & Astronomy, The University of Western Ontario, London, ON, N6A 3K7, Canada

[14]Department of Physics and Trottier Space Institute, McGill University, 3600 University Street, Montreal, QC H3A 2T8, Canada

[15]Magellan Aerospace, 3160 Derry Road East, Mississauga, Ontario L4T 1A9, Canada

[16]Institute for Computational Astrophysics and Department of Astronomy and Physics, Saint Mary's University, 923 Robie Street, Halifax, NS B3H 3C3, Canada

[17]Canada–France–Hawaii Telescope Corporation, Kamuela, HI 96743, USA

[18]Canadian Space Agency, 6767 Route de l'Aéroport, Saint-Hubert, QC J3Y 8Y9, Canada

[19]Department of Physics & Astronomy, Bishop's University, Sherbrooke, QC J1M 1Z7, Canada

[20]Centre for Electronic Imaging, Department of Physical Sciences, The Open University, Milton Keynes MK7 6AA, UK

[21]Department of Physics & Astronomy, University of British Columbia, 6224 Agricultural Road, Vancouver, BC V6T 1Z1, Canada

[22]Department of Physics & Astronomical Science, Central University of Himachal Pradesh (CUHP), Dharamshala, 176215, India

[23]Cahill Center for Astronomy and Astrophysics, California Institute of Technology, MC 249-17, Pasadena, CA 91125, USA

[24]Department of Physics & Astronomy, McMaster University, Hamilton, ON L8S 4L8, Canada

[25]IPAC, California Institute of Technology, Pasadena, CA 91125, USA

[26]Institute for Astronomy, University of Edinburgh, Royal Observatory, Edinburgh EH9 3HJ, UK

[27]Space Astronomy Research Group – AEGORA, Fac. CC Matemáticas, Universidad Complutense, Madrid, Spain

[28]Institute of Cosmology & Gravitation, University of Portsmouth, Portsmouth, PO1 3FX, UK

[29]McWilliams Center for Cosmology, Department of Physics, Carnegie Mellon University, Pittsburgh, PA 15213, USA

[30]Los Alamos National Laboratory, Los Alamos, NM 87545, USA

[31]School of Physics and Astronomy, University of Birmingham, Edgbaston, Birmingham B15 2TT, UK

[32]Inter University Centre for Astronomy and Astrophysics, Ganeshkhind, Pune 411007, India

[33]Teledyne e2v, 106 Waterhouse Lane, Chelmsford, CM1 2QU, United Kingdom

[34]Aix Marseille Univ., CNRS, CNES, LAM, rue Frédéric Joliot-Curie, 13388 Marseille cedex 13, France

[35]Department of Computer Science, Math, Physics, & Statistics, University of British Columbia, Okanagan Campus, Kelowna, BC V1V 1V7, Canada

[36]Astrophysics Research Centre, Queen's University Belfast, Belfast, BT7 1NN, UK

[37]Astronomy Department, University of Michigan, 1085 South University Avenue, Ann Arbor, MI 48109, USA

[38]Department of Astronomy, Indiana University, Bloomington, Indiana 47405, USA

[39]Center for Interdisciplinary Exploration and Research in Astrophysics, Northwestern University, Evanston, IL 60201, USA

[40]Indian Institute of Astrophysics, Koramangala, Bangalore 560034, Karnataka, India

[41]Department of Physics and Astronomy, The Johns Hopkins University, Baltimore, MD 21218, USA

[42]Laboratory for Atmospheric and Space Physics, Boulder, CO, USA

[43]Space Telescope Science Institute, 3700 San Martin Drive, Baltimore, MD 21218, USA

[44]Physics Department, University of Oxford, Denys Wilkinson Building, Oxford OX1 3RH, UK

[45]School of Physics and Astronomy, University of Leicester, Leicester LE1 7RH, UK

[46]Department of Physics and Astronomy, University of Sheffield, Hounsfield Road, Sheffield S3 7RH, UK

[47]International Centre for Radio Astronomy Research – Curtin University, GPO Box U1987, Perth, WA 6845, Australia

[48]Department of Physics and Astronomy, Dartmouth College, 6127 Wilder Laboratory, Hanover, NH 03755, USA

[49]Department of Physics, Université de Montréal, Montréal, QC H2V 0B3, Canada

[50]David A. Dunlap Department of Astronomy & Astrophysics and Department of Statistical Sciences, University of Toronto, Toronto, ON M5S 3G3, Canada

[51]School of Physics, University College Dublin, Belfield, Dublin 4, D04 V1W8, Ireland

[52]Department of Physics, University of Warwick, Coventry, CV4 7AL, UK

[53]Physical Research Laboratory, Ahmedabad, 380009 Gujrat, India

[54]School of Physics and Astronomy, University of Southampton, Southampton SO17 1BJ, UK

[55]DIRAC Institute, Department of Astronomy, University of Washington, 3910 15th Avenue NE, Seattle, WA 98195, USA

[56]National Astronomical Observatory of Japan, National Institutes of Natural Sciences, 2-21-1 Osawa, Mitaka, Tokyo 181-8588, Japan

[57]Department of Astronomy, Yonsei University, 50 Yonsei-ro, Seodaemun-gu, Seoul 03722, Republic of Korea

[58]Department of Physics, University of Winnipeg, Winnipeg MB, R3B 2E9, Canada

[59]FNRS/Université de Liège, B-4000 Sart Tilman, Liège, Belgium

[60]Center for Astrophysics, Harvard & Smithsonian, 60 Garden Street, Cambridge, MA 02138, USA

[61]Department of Physics, Drexel University, 3141 Chestnut Street, Philadelphia, PA 19104, USA

[62]Département de physique, de génie physique et d'optique, Université Laval, 1045 Av. de la Médecine, Québec, G1V 06A, Canada

[63]Physics Department, University of Alberta, CCIS 4-183, Edmonton, AB T6G 2E1, Canada

[64]Department of Physics and Astronomy, York University, 4700 Keele Street, Toronto, ON M3J 1P3, Canada

[65]Department of Physics, University of Bath, Claverton Down, Bath BA2 7AY, UK

[66]The School of Electrical Engineering and Computer Science, University of Ottawa, 75 Laurier Ave E, Ottawa, ON K1N 6N5, Canada

[67]Department of Science, Technology and Society, Division of Natural Science, York University, 4700 Keele St, Toronto ON M3J 1P3, Canada

[68]Department of Astronomy and Yonsei University Observatory, Yonsei University, Seoul 03722, Republic of Korea

Abstract. CASTOR is a proposed wide-field ($30' \times 30' = 0.25$ deg^2), nearly diffraction-limited (FWHM $\sim 0.15''$), 1m-diameter space telescope that is under development by the Canadian Space Agency and the National Research Council of Canada. Optimized for UV/blue-optical wavelengths, the telescope uses dichroics to enable imaging in three channels (and up to five bands) that cover the 0.15 to 0.55 μm spectral region, simultaneously. CASTOR will also feature low- and medium-resolution spectroscopic capabilities through the use of a deployable grism for low-resolution ($R \lesssim 420$) slit-less spectroscopy in its UV and u channels, and medium-resolution $R \sim 1400$ multi-object spectroscopy in a parallel field using a digital micro-mirror device. High-speed, precision photometry will be possible using dedicated CMOS detectors in each of its three channels. This paper presents an overview of the mission, including the optical design, instruments and detectors, payload layout, satellite bus, orbit and ground segment. We describe the mission's scientific capabilities and expected place within the astronomical landscape in the 2030s. The 5-year lifetime is baselined to a combination of legacy surveys, guest observer programs and target-of-opportunity science. We summarize scientific plans for the mission in each of eight fields: cosmology; time domain and multi-messenger science; active galactic nuclei; galaxies; near-field cosmology; stellar astrophysics; exoplanets; and solar system studies. We conclude by describing ongoing development efforts, highlighting areas of particular relevance for NASA's Habitable Worlds Observatory.

*Patrick Côté patrick.cote@nrc-cnrc.gc.ca

1 Introduction

The Ultraviolet-Optical-Infrared (UVOIR) region can be loosely defined as the wavelength range from 0.0912 μm (the Lyman edge of HI, below which the interstellar medium is opaque) to ~ 5 μm (above which water absorption in the atmosphere makes ground-based observations nearly impossible). As is well known, most of the emission from stars and gas in the nearby universe is emitted in a broad peak centered in this UVOIR region, with a second peak in the far-IR caused by dust emission from reprocessed stellar photons. The UVOIR is thus fundamental to the study of stars, galaxies, planets, the intergalactic medium, the interstellar medium, and active galactic nuclei. The UV end of this wavelength interval is especially rich in astrophysical information since it is in this region that radiation and matter interact most strongly, via atomic ionization and recombination processes and the stimulation and dissociation of molecules.

1.1 Ultraviolet and Optical Astronomy: Why Observe from Space?

Because the Earth's atmosphere absorbs and scatters photons in the so-called "vacuum UV" band (between 0.091 and 0.32 μm), the study of astrophysical sources in this wavelength region requires observations conducted from space. In fact, there are a number of reasons to prefer space-based platforms for wide-field imaging and spectroscopy at UV *and* optical wavelengths:

- **Direct Access to the Ultraviolet Region**. Below ~ 0.32 μm, the atmosphere is almost entirely opaque due to the combination of ozone absorption and Rayleigh scattering, and absorption can still be significant in the 0.32 to 0.4 μm range. Observing from space provides direct access to this UV/blue-optical region.

- **Image Sharpness and Atmospheric Turbulence**. Light from astronomical sources that passes through the Earth's atmosphere undergoes turbulent mixing, blurring the source image. Even at the best ground-based sites, the full width at half maximum (FWHM) of this seeing disk is typically no better than $\sim 0.''7$. The development of adaptive optics systems on ground-based telescopes can

improve image quality, but such gains are typically realized over small fields, usually only at wavelengths longer than ∼0.5 μm, and come at the cost of spatially and temporally varying point spread functions (PSFs).

- **Photometric Calibration and PSF Stability**. The photometric precision achieved in astronomical surveys is often limited by systematic errors in the calibration (e.g., changes in system throughput or zero-point, flat-field corrections, etc) or the spatial and temporal stability of the PSF. With proper care, space telescopes can deliver sharp, stable PSFs and accurate photometric calibrations.[1–3]

- **Low Backgrounds**. At ground-based sites, moonlight scattered by the atmosphere can sharply increase sky brightness at short wavelengths so that deep blue-optical imaging is only possible during periods of low lunar illumination. Even then, varying atmospheric conditions can make accurate photometric calibration challenging. From space, it is possible to capitalize on the dark and uniform backgrounds at short wavelengths. Indeed, it is in the UV region that astrophysical sources often have their greatest contrast against the underlying background.

There are some technical considerations that link the design and development of observing facilities across the UVOIR range including the widespread use of silicon-based detectors that operate by converting incoming photons into electric charge. However, there are no fundamental obstacles involved in building telescopes that operate over the full UVOIR region, and the Hubble Space Telescope (HST) — the most famous and productive UVOIR telescope in history — was designed with the above considerations in mind.

Launched in 1990, HST has now exceeded its design lifetime, and the next generation of high-resolution space telescopes are focusing on red-optical and IR wavelengths: i.e., JWST, Euclid and Roman. However, the scientific motivation for continued access, from space, to the full UVOIR region remains very strong. The Astro2020 decadal review recommended the Habitable Worlds Observatory (HWO) as NASA's future flagship observatory.[4] Like HST, HWO will carry out observations spanning the full UVOIR region. With an expected launch date in the 2040s, NASA has established the Great Observatory Maturation Program to mature the technologies needed for this ambitious mission. A large fraction of the technologies requiring technology readiness level (TRL) advancement involve the UV and blue-optical region.[5]

In what follows, we describe the proposed CASTOR (*Cosmological Advanced Survey Telescope for Optical and ultraviolet Research*) mission. The original concept dates to a 2012 study that examined the science case for such a facility and presented a preliminary design.[6] Following a series of technology development studies carried out in the mid-2010s,[7,8] and a 2019 study to update the science mission,[9,10] the project was selected in the 2020 Long Range Plan for Canadian Astronomy as the highest priority among very large investments in space astronomy.[11] The mission design, science program, partnership scenarios, schedule, and development plan were subsequently advanced in overlapping Phase 0 and Space Technology Development Program (STDP) studies carried out between 2021 and 2024. In this article, we briefly summarize the current design and expected performance of the mission, including an overview of ongoing development activities. At the time of writing, the mission team is hoping to move to Phase A in 2025.

Table 1 Comparison of Notable UV/Optical Space Missions

	HST/WFC3[a]	GALEX[12]	UVIT[13]	Ultrasat[14]	UVEX[15]	CASTOR
Launch	2009	2003	2015	2027	2030	2031
Duration (yrs)	>15	2.5 (planned) 11 (actual)	5 (planned) >9 (actual)	>3	2	>5
Aperture (cm)	240	50	37.5	33	75	100
FoV (deg^2)	0.002	1.1	0.17	204	12.25	0.25
Wavelengths (nm)	200-1000	135-275	180-300	230-290	139-270	150-550
Imaging bands (nm)	Long-pass (4) Extremely Wide (2) Wide (12) Medium (9) Narrow (35)	135-175 (FUV) 175-275 (NUV)	130-180 (5 FUV) 200-300 (6 NUV) 320-550 (5 VIS)	230-290 (NUV)	139 – 190 (FUV) 203 – 270 (NUV)	159 – 292 (UV) 294 – 404 (u) 396 – 554 (g) 223 – 292 (UV^L) 294 – 353 (u^S)
FWHM ($''$)	0.08-0.07	4.5, 5.5	1.5	8.3	<2.25	0.15
Sens. 5σ (1000s)	27.3 (U)	23.5	21.7 (FUV) 23,5 (NUV)	22.6 (NUV)	24.6 (FUV) 24.6 (NUV)	27.5 (UV) 27.4 (u) 27.0 (g)
⟨ToO response time⟩		0		<15 min	<3 hrs	<3 hrs

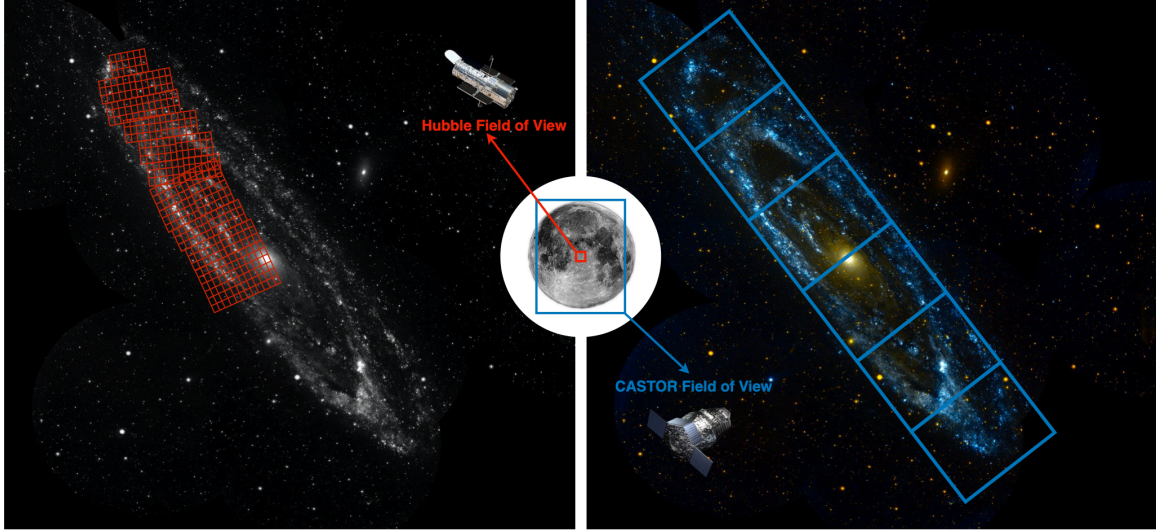Notes: a – https://www.stsci.edu/hst/instrumentation/wfc3

Fig 1 A comparison of CASTOR's field of view to that of the Hubble Space Telescope (HST) overlaid on an ultraviolet image from GALEX.[12] The figure on the left shows the distribution of HST fields from the Panchromatic Hubble Andromeda Treasury (PHAT) — one of the largest programs carried out with HST and the most comprehensive existing study of the Andromeda galaxy (M31). PHAT covered approximately a third of M31's disk with 414 separate pointings, shown in the panel to the left, each of which was imaged six times in six different filters over a 40-day campaign.[16] The figure on the right shows how CASTOR could map the entirety of Andromeda's disk in six pointings. The different HST and CASTOR fields are superimposed on the full moon, which is shown to scale at the center of the image.

1.2 *Context within the International Landscape*

To put the mission in context, Figure 1 presents a comparison between CASTOR and HST. The panel on the left shows a mosaic GALEX image of M31[1] with the distribution of HST fields from the Panchromatic Hubble Andromeda Treasury (PHAT) superimposed. This 828-orbit survey mapped the UVOIR emission from a region covering roughly a third of the M31 optical disk.[16] On the right, we show how the entire M31 disk could be mapped with six CASTOR fields, thanks to its ∼100× larger field of view. Figure 2 shows how CASTOR would complement the data from other high-resolution space telescopes (JWST, Euclid and Roman) by providing access to the UV/blue-optical region.

Space-based access to the UV skies is also the prime motivation for several upcoming time domain and multi-messenger (TDAMM) space missions (e.g., Ultrasat,[14] UVEX[15]). These missions, however, are optimized for ultra-wide fields rather than high angular resolution so CASTOR will be highly synergistic with these facilities as well.[2] Table 1 presents a high-level comparison between CASTOR, Ultrasat, UVEX, as well as some notable earlier UV/optical instruments and missions (i.e., the WFC3/UVIS camera aboard HST, GALEX and the UVIT instrument aboard Astrosat). CASTOR occupies a unique place among previous and upcoming missions, having a sensitivity and resolution comparable to HST but with a field of view similar to Euclid or Roman.

As described below, CASTOR's science mission will feature a range of high-impact programs with broad appeal (see §4). It will deliver the widest, deepest, sharpest view of the UV/blue sky ever produced, and perform a comprehensive study of star formation within nearby galaxies and across the history of the Universe. Short-wavelength imaging and spectroscopy will provide unique information on the early-time

---

[1]Credit: NASA/JPL-Caltech

[2]Compared to CASTOR, Ultrasat and UVEX have fields of view that are larger factors of ∼800 and ∼80. In terms of encircled energy, CASTOR's "seeing disk" is smaller by factors of ∼3000 and ∼200.
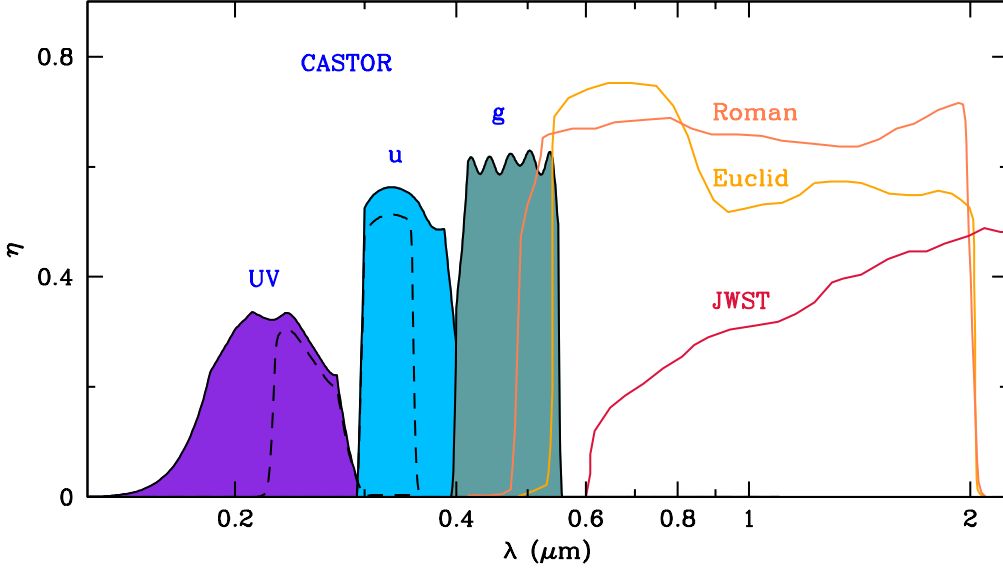
Fig 2 Total system throughput, η, versus wavelength for several high-resolution space telescopes. CASTOR will complement red-optical/IR imaging from JWST, Euclid and Roman. Its wide-field imager uses dichroics to provide simultaneous three-band imaging over the 0.15 to 0.55 μm wavelength range. A deployable broadband filter allows users to subdivide the UV and u channels (dashed curves).

UV emission from astrophysical transients, including electromagnetic counterparts to gravitational wave events. The mission will map the growth of supermassive black holes in galaxies over a period of 10 billion years. By mapping the Milky Way's disk, bulge, stellar streams and satellite galaxies, it will shed light on the formation of the hottest, youngest and most massive stars, the hierarchical assembly of our Galaxy, and the structure of dark matter halos on the smallest scales. It will probe the atmospheres of exoplanets, including the presence of water and hazes, and assess how flares from M stars, the most common type of star in the universe, could affect the survival of life on orbiting exoplanets. It will map the smallest and most distant objects in our Solar System and characterize their surface chemistry, including organic compounds.

The development of the mission has been led by the Canadian Space Agency (CSA), National Research Council of Canada (NRC), a consortium of aerospace companies (Honeywell Aerospace, ABB Ltd, Magellan Aerospace), and a broad network of scientists based at universities and research institutes across the globe. Technical and scientific development has also benefited from contributions by international collaborators, such NASA's Jet Propulsion Laboratory and the California Institute of Technology, including contributions from JPL's Microdevices Laboratory-MDL, as well as scientists and engineers based in the United Kingdom, with support from the UK Space Agency (UKSA), and in the USA, India, France, Spain and elsewhere.

This paper is organized as follows. In §2, we describe the current design of the spacecraft, including the payload, telescope, instruments, bus, launch, orbit, and ground stations. In §3, we discuss the science program and present a summary of the candidate legacy surveys developed by the science team during the recently completed Phase 0 study. In §4, we provide more details on the mission's anticipated scientific impact for each of eight Science Working Groups, from cosmology to the solar system. In §5, we describe development activities that are underway in the lead-up to the possible start of a Phase A study in 2025; we also note how some of these activities align with technology development for the HWO mission. We conclude and summarize in §6.
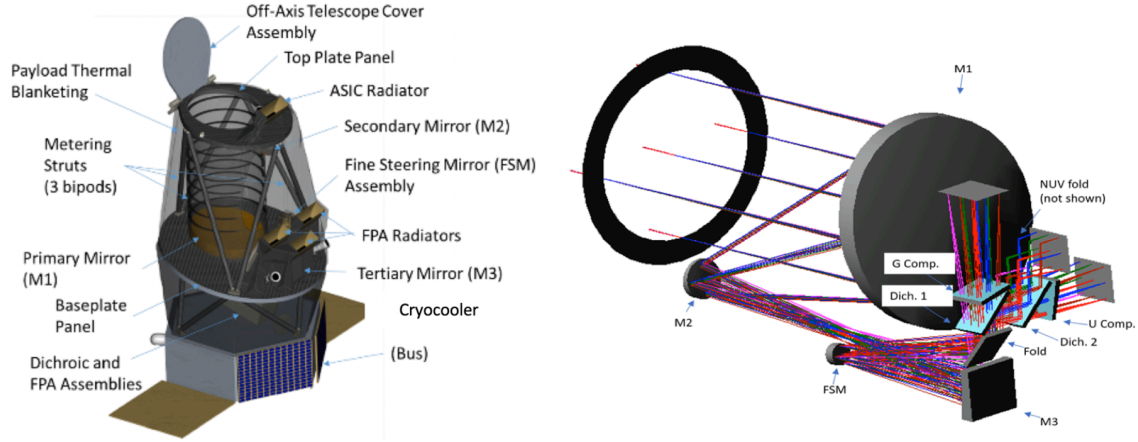
Fig 3 (Left) Illustration of the main payload elements for the telescope (see §2.1, §2.2 and §2.5 for details). (Right) Schematic diagram showing the opto-mechanical design of the telescope. An off-axis, three-mirror anastigmat design uses a fine steering mirror for image stabilization and two dichroics to direct the incoming light onto three focal plane arrays (FPAs).

2 Design

In this section, we give a brief description of the mission design including the payload; telescope and assembly; instrument suite; guider and fine steering mirror; choice of orbit; launch vehicle options; and ground station networks. A summary of the mission and its various instruments and observing modes is presented in Table 2.

2.1 Hardware Layout

The overall hardware layout is shown in the left panel of Figure 3. The spacecraft will use a small-SAT panel design with a hexagonal bus structure. The bus module's primary structure consists of a clampband interface adapter, thrust cone and shear struts. Most bus units are mounted to the side panels. The payload structural design utilizes a top structure (for M2) held off the baseplate (for M1) by metering struts as well as a mid-panel. The telescope mirrors are currently baselined to be light-weighted Zerodur low-expansion glass. The backbone of the telescope payload is the support structure which consists of a baseplate panel, a top plate panel and metering bipods. The panels are baselined to be of the honeycomb type with carbon fiber reinforced polymer (CFRP) facesheets and aluminum honeycomb core of various densities. A telescope cover assembly utilizes a panel similar in construction to the CFRP honeycomb panels of the support structure combined with a motor-driven deployment mechanism. The main baffle will be circular and supported on the metering struts, with baffles used to shroud the M2 path.

2.2 Telescope and Payload Opto-Mechanical Subsystems

An unobscured Three Mirror Anastigmat (TMA) telescope with a 1m-diameter primary mirror delivers an image quality of FWHM $\lesssim 0.15''$ over a wide field (i.e., roughly half a degree in diameter). This optical design (see the right panel of Figure 3) provides nearly diffraction-limited performance over this full field, with a field stop for stray light control and a real exit pupil for thermal control. Channel separation is provided by two dichroics that separate the incoming light at wavelengths of ~ 0.3 μm and ~ 0.4 μm. The design includes transmissive elements in two bands so transmissive wedges are used to correct chromatic aberration. Bandpasses are defined by the dichroics, broadband dielectric coatings on the mirrors (M1, M2, M3 and FSM) and multi-layer anti-reflection coatings on the detectors. An M2 focus mechanism is
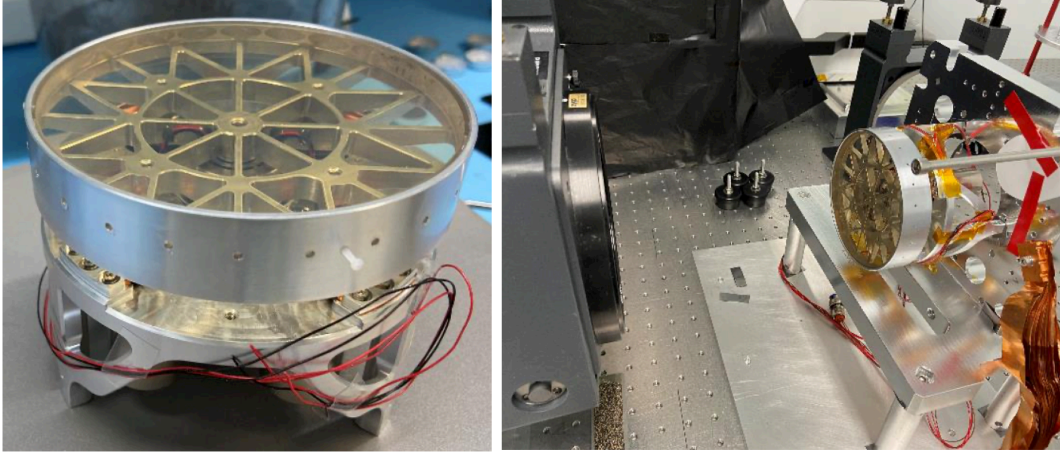
Fig 4 Zerodur fine steering mirror (FSM) prototype, without reflective coating, undergoing wavefront error testing at the ABB Measurement and Analytics facility in Quebec City. The fully functional FSM tip-tilt mechanism is mounted on a damped optical table, in front of a Zygo interferometer. See §2.3 for details.

composed of three individual mechanisms mounted on a common frame. The mechanism will allow for minor tip/tilt adjustment by employing differential movements of the three linear actuators.

An off-axis design was adopted over an on-axis approach since it provides a more desirable diffraction pattern by avoiding the center obscuration and supporting spiders of the secondary (i.e., the PSF of an unobscured image has a higher peak and fainter diffraction rings). In terms of stray light control, the off-axis design is preferred due to the absence of spider scattering and a shorter front baffle with inner walls between mirrors.

2.3 Guider and Fine Steering Mirror

During science imaging, the spacecraft must maintain an inertially-fixed three-axis orientation, with the telescope boresight pointed directly at the celestial target, and zero nominal rotation about that axis. In practice, disturbances on the spacecraft will prevent perfect pointing, and to achieve the subarcsecond limit on image jitter during exposures, the telescope optics include a fine steering mirror (FSM) operating at high frequency, with guide star images used to correct for short-term spacecraft movement (on a timescale of fractions of a second). Figure 4 shows a prototype of the FSM during wavefront error testing. Guiding will be performed using two CIS120 sensor chip assemblies (SCAs) located at the corners of the g-band focal plane array (FPA) to compensate for roll (Figure 5). These star tracking SCAs are identical to the precision photometer SCAs (see below) which allows a layer of redundancy in the attitude and orbit control system design.

2.4 Science Instruments

A schematic view of CASTOR's instrument suite is shown in Figure 5. We briefly describe each of these instruments and observing modes below.

2.4.1 Wide Field Imaging and Slit-less Spectroscopy

CASTOR's primary instrument is a wide-field imager for high resolution imaging in the UV/blue-optical region. A pair of dichroics and wedge filters are used to divide the incoming light into three imaging channels that cover the UV (0.15–0.3 μm), u (0.3–0.4 μm) and g (0.4–0.55 μm) passbands, simultaneously.[17] Each focal plane is mosaicked with a 2×2 array of CMOS devices having 10 μm (0.1″) pixels.
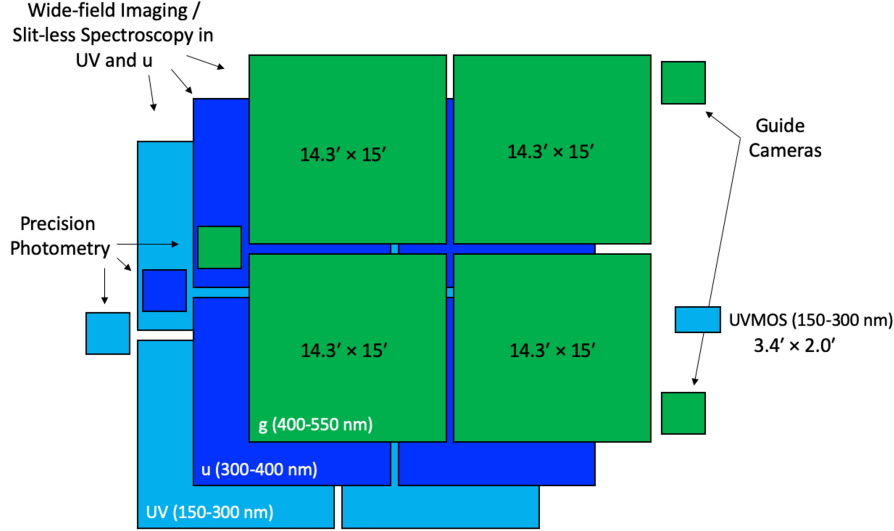
Fig 5 A schematic view of CASTOR's instrument suite. Simultaneous wide-field imaging in the UV, u and g passbands is enabled by dichroics that divide the incoming light into three channels covering the 0.15 to 0.55 μm range. A deployable grism provides low-resolution ($300 \lesssim R \lesssim 420$) slit-less spectroscopy over the full imaging field, in the UV and u channels. Each of CASTOR's three focal plane arrays (FPAs) is accompanied by a dedicated CMOS detector for high-precision photometric measurements of transiting exoplanets. Medium resolution long-slit and multi-slit spectroscopy is possible using a UVMOS instrument that observes an adjacent field. Two CMOS devices in the $g-$band channel provide spacecraft guiding.

The choice of detector is fundamental as many science programs (Table 3) require high quantum efficiency, low readnoise, low dark current, large fields and small pixels. In addition, the selected device should be compatible with the power resources of a small satellite bus and have low power dissipation on the focal plane in order to stay within the cooling and power budget. Following extensive detector assessment efforts, the CIS300-series large-format, back-thinned CMOS detectors from Teledyne-e2v were selected. These devices measure 9000×8600 with 10 μm pixels so that the 2×2 array in each channel covers an area of $0.\!\!^\circ485 \times 0.\!\!^\circ508 \approx 0.239$ deg^2 (excluding $\sim 26''$ gaps between adjacent devices). The expected readnoise and (beginning of mission) dark current are 3 e^- px^{-1} and 10^{-4} e^- s^{-1} px^{-1}, respectively, although these values will need to be verified by laboratory measurements (see §5.3). Similarly, the full well depth and linearity range of the detectors will need to be characterized in the laboratory; for reference, the predicted full well depth of 140,000 e^- in low gain mode corresponds to saturation magnitudes in the range 11.1–11.4 mag for a 1 sec exposure.

The FWHM in each channel is roughly $0.\!\!''15$. Because the PSFs (shown in Figure 6) are slightly undersampled by the $0.\!\!''1$ pixels, most imaging programs will be carried out using a combination of small and/or large dithers to fill detector gaps and adequately sample the PSF.

A deployable filter with a central wavelength of ~0.3 μm and full width ~0.12 μm may be inserted (between the dichroics) to divide the light in the UV and u channels for finer sampling of the spectral energy distribution of astrophysical sources. This same mechanism can also be used to insert a grism for low-resolution, slit-less spectroscopy over the full imaging field. A single grism provides a resolving power R between 280 and 360 in the UV channel, and 360 to 460 in the u channel.

2.4.2 Precision Photometers

Each of the three FPAs includes a single CMOS detector optimized for high-speed observations of transiting exoplanets (Figure 5, §4.7). The photometer SCAs can be integrated onto the same mosaic FPA mounting
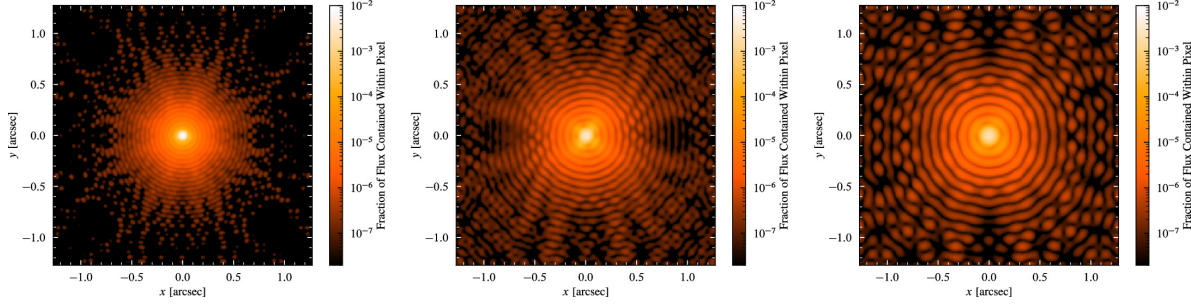
Fig 6 Point spread functions (PSFs) at the field center in each of CASTOR's UV, u and g channels (left to right, respectively).[17]

structure as the main scientific FPAs and remain in focus.

The photometer detectors are currently baselined as the Teledyne-e2v CIS120 back-illuminated CMOS array with 2048×2048 pixels at $0\rlap{.}{''}1$ pitch. Anticipated frame rates are 20 fps full frame and up to 82 specified half rows at 1 kHz. The CIS120 detectors make it possible to capture multiple "regions of interest", with minimum sizes of 20×20 pixels, for both target object and adjacent reference stars in the 11 arcmin^2 field of view. The need for a diffuser or Fabry lens will be examined in future design studies.

2.4.3 UV Multi-Object Spectrograph

Given CASTOR's 1m aperture and UV sensitivity — and the expected community interest in UV spectroscopic capabilities during the period between the end of HST operations and the launch of HWO — a medium resolution ($R \sim 1400$) spectroscopic capability for the UV region is under consideration (see §5.4). This instrument would be located adjacent to the UV FPA and offer a multi-object spectroscopic capability in a field offset by $\sim 4'$ from the main imaging arrays. The (compact) instrument currently uses an Offner-type design with two concave mirrors, a convex grating with 1190 lines/mm and a digital micro-mirror device (DMD) as the object selector. The field of view is set by the DMD size; currently, the design is baselined to the TI DLP9500 DMD with dimensions 20.7 x 11.7 mm (or $217'' \times 117''$). The large number of elements, and small size of the individual mirrors, are well suited to spectroscopic observations that require high spatial resolution, such as sources in dense environments. The spectrograph design gives a spectral resolution of $R \sim 1000$ between 150-300 nm, or roughly double that over a restricted wavelength range of 180–300 nm.

2.5 Spacecraft Bus

The satellite bus is responsible for providing attitude control; command and data handling; command and control communications with the ground segment; electrical power during the mission to support payload operations; and the structural support needed to protect the ~ 630 kg payload from the stresses of launch and orbit insertion. CASTOR is baselined to the customizable MAC-200 small-SAT bus by Magellan Aerospace which has been flight-proven on various missions, including CASSIOPE (Cascade Small-sat and Ionospheric Polar Explorer) launched in 2013 and the RADARSAT Constellation Mission launched in 2019 (Figure 7).

Key bus design drivers for CASTOR are attitude determination and control (due to the need for low jitter during imaging), telemetry downlink, and structure and layout (to keep the spacecraft compatible with launch vehicle options). Input power will be provided by four solar arrays: two body-mounted and two deployable (see the left panel of Figure 3). This system will provide sufficient power for nearly all science attitudes, except near the ecliptic poles at the solstices during peak power draws. A heritage battery with a capacity of 36 Amp-hours will provide power during such cases. Power will be distributed to the bus and payload by Magellan's Power Control Unit.

Fig 7 CASTOR will be mounted on the MAC-200 satellite bus from Magellan Aerospace Corporation. This bus is pictured during assembly of the Radarsat Constellation Mission which launched in 2019. For more details, see §2.5.

2.6 Launch and Orbit

A range of orbits were considered for the mission, each with their own advantages and disadvantages. In the end, a circular, sun-synchronous low earth orbit (LEO) with an inclination of $98.6°$ and altitude ~800 km was adopted. A "dawn-dusk" configuration is preferred over "dusk-dawn" (although either can be supported) given the former's slightly higher observing efficiency for southern targets (such as LSST and Roman survey fields). This choice of orbit allows for efficient observing in the anti-Sun direction with minimal earth occultations and has good ground link opportunities — and correspondingly short (≤ 3 hr) target-of-opportunity response times. Moreover, this orbit is achievable with a variety of launchers (e.g., PSLV, Falcon 9, Nuriho, etc) and has a more favorable radiation environment than Medium Earth or Geostationary orbits. A final selection of launch vehicle will be made in the next phase of mission development.

The continuous viewing zone (CVZ) for this choice of orbit is a conical region of sky centered on the orbit anti-normal direction and includes all parts of the sky that are never blocked by the Earth during any part of an individual orbit. As such, the CVZ varies throughout the year and, for an altitude of 800 km, covers an instantaneous area of ~1000 deg^2 for an Earth exclusion angle of $10°$. Over the course of the year, the CVZ sweeps out an area covering roughly a third of the sky.

2.7 Ground Station Networks

Given the high data rates expected for certain programs, the current baseline calls for science data to be downloaded to a network of optical ground stations. A minimum of four geographically-distributed optical ground stations will be required to overcome the obscuration of optical gateways due to unfavorable atmospheric conditions for pre-planned and on-demand requests. This optical network will include a recently installed facility in Gatineau, QC; another such station could be located at Inuvik Satellite Station Facility, NT, whose high latitude ($68°.4$ N) is well suited to CASTOR's near-polar orbit. Download speeds of ~10 Gbps will be sufficient for the currently envisioned science programs (Table 3). Additional optical ground stations would be accessed either through newly developed facilities, interagency (partner) networks, or commercial networks. Although an optical downlink network is the current baseline, a reevaluation of this choice (including a trade study for optical vs. radio wavelengths) is planned during the Phase A study.
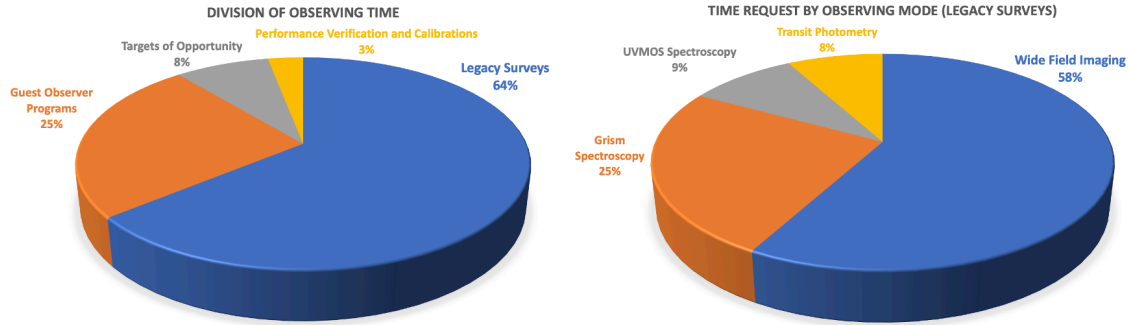
Fig 8 (Left) Preliminary division of observing time recommended in the Phase 0 study; see §3 for details. (Right) Division of observing time by instrument for the 14 candidate legacy surveys from the Phase 0 study and summarized in Table 3. Surveys will be refined in subsequent phases according to developments in the international astronomy landscape and partner requirements.

Routine control, monitoring, and communication with the space system will be provided by the Ground Station Network for S-Band Telemetry, Tracking and Commanding which consists of radio frequency stations distributed across Canada and in TrollSat, Antarctica. Based on a link assessment around the summer solstice, only two contact gaps in excess of 90 minutes were identified, meeting the requirement for most target-of-opportunity programs.

3 Science Program and Division of Observing Time

A fundamental issue in defining the science program is the choice of operations model. Some previous missions have operated largely as experiments, performing surveys or conducting a set of measurements (e.g., WMAP, Planck, Kepler, TESS, Euclid). Others have operated chiefly as Guest Observer (GO) facilities (e.g., HST, Chandra, Astrosat, JWST). A third model adopts a hybrid approach, carrying out large surveys while reserving a fraction of time for GO programs. Examples in this case include GALEX, Spitzer, Herschel, and Roman.

CASTOR will use this hybrid approach, devoting the majority of the observing time to legacy surveys (62%) and reserving a fraction of time for GO programs (25%). Note that legacy surveys are distinguished from GO investigations by the criteria defined by the Spitzer mission: i.e., they are:

- large and coherent science projects, not reproducible by any reasonable number or combination of smaller GO investigations;

- projects of general and lasting importance to the broad astronomical community with the observational data yielding a substantial and coherent database.

A total of fourteen candidate legacy surveys were developed during the Phase 0 study (and listed in Table 3). More information on these programs is given in §4 which discusses science drivers in detail. Some observing time will also be reserved for target-of-opportunity (ToO) observations (8%) while a smaller fraction of time will be taken up by performance verification and calibrations (3%). This overall breakdown, which will be revisited during future development phases, is illustrated in the left panel of Figure 8.

As discussed in §2, CASTOR will offer several options for observing mode. The breakdown of time requested by these 14 candidate legacy surveys is shown in the right panel of Figure 8. More than half of the time required for these surveys utilizes the wide-field imagers (58%). Roughly a third of the time relies on spectroscopic observations, either slit-less spectroscopy using the deployable grism (25%) or UVMOS instrument (9%). Photometric monitoring of transiting exoplanets accounts for the remaining 8% of the time. It is expected that these numbers will change when the legacy surveys are revisited in the next development phase.

13

Table 2 CASTOR Mission Summary

Primary aperture	1m off-axis, un-obscured, light-weighted Zerodur
Lifetime	5 years minimum, with possible extended lifetime
Orbit	Low-earth, sun-synchronous, dawn-dusk orbit ($\sim$800 km, 98° inclination)
Operational modes	1. wide field imaging in three channels simultaneously
	2. precision photometry
	3. slit-less spectroscopy in UV and u channels, simultaneously (full field)
	4. multi-slit, medium resolution UV spectroscopy in parallel field
Wide Field Imaging (WFI)	
Imaging field of view	0.485° x 0.508° = 0.247 deg^2 (fill factor = 96.7%)
Image quality	FWHM $\approx 0.15''$ in all channels
Baseline detector	T-e2v CIS301 9k×8.6k detectors with 10 μm (0.1$''$) pixels. 2×2 arrays per channel, 12 in total
Photometric channels	1. UV (150-300 nm)
	2. u (300-400 nm)
	3. g (400-550 nm)
Spacecraft orientation	Telescope points $> 90°$ from sun. Target fields are in the anti-sun direction
Data volumes	$\lesssim$ 600 GB/day
Downlink	High-speed optical downlink ($\sim$10 Gbps)
Precision Photometry	
Photometric channels	Same as WFI: UV, u and g
Combined differential photometric precision	$\leq$ 50 ppm on a 3-hr timescale for a $g = 10$ G2V star
Duty cycle	$\geq$ 90% for 1-minute integrations
Grism Spectroscopy	
Spectroscopic field	0.485° x 0.508° = 0.247 deg^2 [full imaging field of view]
Spectroscopic channels	1. UV (150-300 nm)
	2. u (300-400 nm)
Resolving power	1. R$\sim$300 in UV channel, $\Delta\lambda$ over 2 px, 1 px = 10 μm
	2. R$\sim$420 in u channel, $\Delta\lambda$ over 2 px, 1 px = 10 μm
Point Spread Function	FWHM $\lesssim 0.2''$ in both channels
UV Multi-Object Spectroscopy	
Spectroscopic field	217$''$ x 117$''$, offset by $\sim$4$'$ from the edge of the imaging field.
Spectroscopic channels	UV (150-300 nm) at R = 700-1400
DMD	TI DLP9500 DMD with 10.8 μm pixels (1920 x 1080)
Spectrograph detector	2.5k×7k CMOS detector with 10 μm pixels (where 0.1$''$ = 10 μm)
Spectral dispersion	10.7 nm/mm at R$\sim$1000
PSF in spatial direction	$\lesssim 0.20''$

Table 3 Candidate Legacy Surveys

ID	Candidate Legacy Survey	SWGs	Area (deg^2) or Targets	Data	Program Notes
1	CASTOR Wide Survey	COS, GAL, NFC, SA, SS	2227	WFI	Roman HLS footprint, two epochs
2	CASTOR CADENCE: A Wide-Field UV Time-Domain	TD, AGN, SA, GAL, COS	10	WFI, grism, UVMOS	Daily cadence, LSST DDFs
3	CASTOR ToO: Rapidly Responding to the Dynamic Universe	TD, SA, NFC, GAL	10	WFI	Rapid response
4	CASTOR AGN Reverberation Mapping Survey	AGN, TD, GAL	10	WFI, grism, UVMOS	Daily imaging, targeted fields are LSST DDP fields
5	CASTOR Nearby Galaxies Survey	GAL, NFC, TD,SA	700 galaxies	WFI	
6	CASTOR Deep and Ultra Deep Imaging Surveys	GAL, COS, TD, AGN, NFC	83	WFI	Survey, map and monitoring program
7	CASTOR Grism Legacy Survey	GAL, COS, AGN, NFC, TD	83	grism	Grism to map the same field of the Deep Survey
8	CASTOR Galactic Substructures Survey	NFC, SA, TD, GAL, COS	276 (90 targets)	WFI, UVMOS	Multiple epochs
9	CASTOR Magellanic Clouds Survey	NFC, SA, GAL, TD	105	WFI, grism, UVMOS	
10	CASTOR Square Kilodegree Galactic Plane Survey	SA, NFC, TD	1075	WFI, grism, UVMOS	
11	CASTOR M Star UV Radiation Environments Survey	SA, EXO	150 (+ 5 targets)	WFI, UVMOS	
12	CASTOR Transit Exoplanet Survey	EXO, SA	22 targets	PP	CVZ targets
13	CASTOR Trans-Neptunian Objects Survey	SS, SA, NFC	2160 (wide) 30 (deep)	WFI, grism	Moving targets
14	Uncovering the Drivers of Cometary Activity	SS	25 targets	grism, UVMOS	ToOs selected from LSST

4 Science Program

In this section, we provide short descriptions of science drivers and opportunities for the mission, as developed by eight science working groups during the recently completed Phase 0 study.

4.1 Cosmology

Stage IV dark energy experiments will survey the skies at optical and IR wavelengths to understand the structure, expansion and geometry of the universe. This is an undertaking beyond any single facility as it requires "perfect datasets"[18] that combine high sensitivity and spatial resolution, wide wavelength coverage and specific observing cadences that depend on the cosmological probe of choice: i.e., weak gravitational lensing, baryon acoustic oscillations, or Type Ia supernovae. CASTOR will add unique information to these surveys due to its focus on the UV/blue-optical region, wide field of view and high angular resolution.

The primary CASTOR legacy survey for cosmology research is the Wide Survey which targets the $\sim$2200 deg^2 region in the southern hemisphere that will be covered in Roman's High Latitude Wide Area Survey (HLWAS; Table 3). The Wide Survey will provide imaging and photometry in multiple passbands covering the 0.15 to 0.55 μm range; observations with, and without, the broadband filter (which divides the UV and u channels) will be collected at two epochs separated by 1-3 observing seasons. Reaching point-source depths of $m_{AB} \simeq 26.5$–27.5, the survey is designed to match the 10-year g-band depth of the Rubin-LSST survey with a roughly 5-fold improvement in angular resolution (Figure 9).

The main survey of the ground-based Rubin Observatory, LSST, will be a photometric imaging survey covering 18,000 deg^2 to image billions of galaxies with hundreds of repeat observations.[19] The addition of CASTOR data will add discrimination power in several areas, including the determination of photometric redshift outliers, deblending of sources at the limit of the ground-based data, galaxy shape measurements, and SED-fitting of astrophysical sources, including strong-lensing systems: e.g.,

- *Photometric redshifts*: CASTOR improves the LSST photo-z estimates across all redshifts by about 10%, and up to 20% at low- ($z < 0.6$) and high- ($z > 2.0$) redshifts. It will do this by breaking degeneracies in the optical colors of low- and high-z galaxies, and more securely identifying galaxies that are truly low-z objects. In addition to improving photo-z accuracy, CASTOR has the potential to reduce outlier fractions at low- and high-z by a factor of two.[20] An information theoretic metric of potentially recoverable redshift information applied to LSST, Euclid, Roman and CASTOR[21] indicates that CASTOR provides similar redshift information to the infrared surveys at $z < 1.5$ and combinations of CASTOR and LSST have similar potentially obtainable redshift information as combinations of LSST and Euclid (see their Figure 4).

- *Source deblending*: The CASTOR PSF[17] is $\sim$5$\times$ sharper than that of LSST in the g-band,[22,23] which will allow it to resolve $\sim$80% of the blends in deep LSST g-band imaging. By reducing ambiguous blends of galaxies at different redshifts, CASTOR will reduce the level of shear noise in lensing surveys and reduce the level of correlated biases between the measured local density, shear and redshift.

- *Galaxy shape measurements*: To use weak lensing to detect cosmic shear, surveys need to detect a distortion of galaxy shapes at the level of approximately 0.01.[24] CASTOR will be able to provide robust shape measurements in the g-band for a significant number of sources. Combining this data with that of the Roman HLWAS will provide improved shape measurements at a catalog level, while multi-filter shape measurements can test for systematic effects. In combination with LSST and Euclid, CASTOR will improve shape measurements and reduce blending, in addition to detecting small and/or faint galaxies not otherwise detectable.
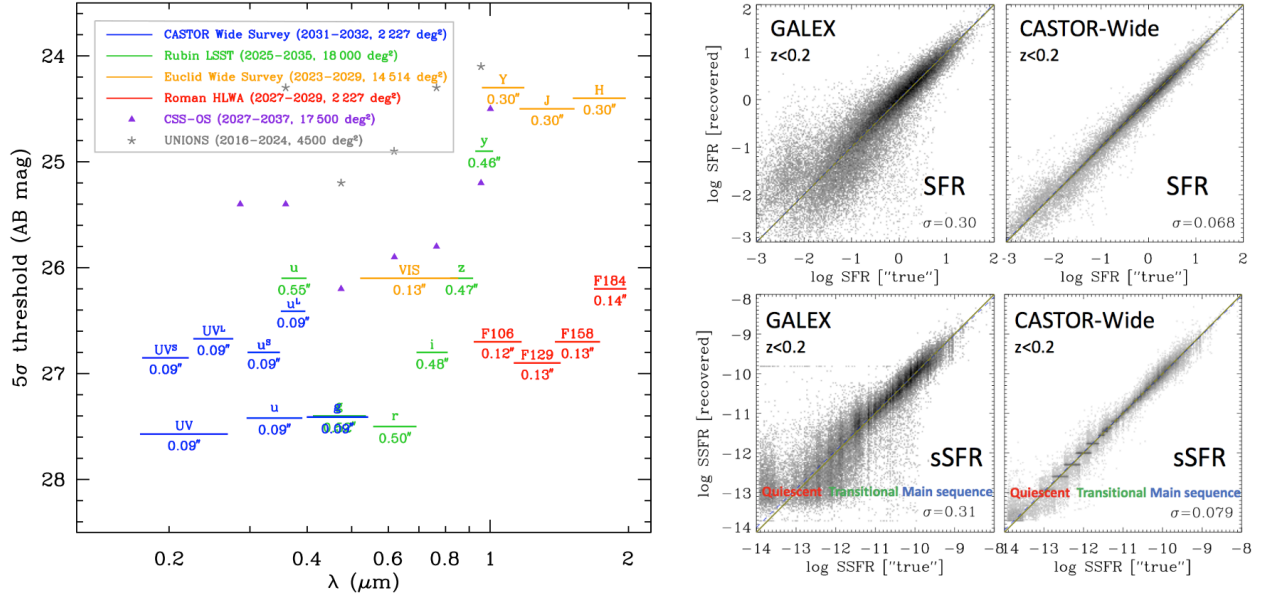
Fig 9 (Left) Depths of wide-field UV/optical/IR imaging surveys plotted as a function of wavelength. Results are shown for several survey: UNIONS,[27] LSST,[19] Euclid-Wide,[25] Roman-HLWA,[28] CSS-OS[29] and CASTOR Wide. Note that CASTOR Wide targets the same footprint as the Roman HLWA survey. The labels under each filter indicate the survey's approximate image quality (i.e., EE50 radius). (Right) Predicted improvements in the determination of SFR (upper panels) and specific SFR (lower panels) from the CASTOR Wide Survey (right panels) compared to the GALEX Medium-Deep Survey (left panels). The gains are most dramatic for quenching galaxies located in the transitional zone (i.e., the Green Valley).

- *Strong lensing SED and lens modeling*: CASTOR's angular resolution will allow it to improve strong lensing modeling for systems observed by LSST and Euclid, and by providing UV/blue-optical data, will contribute to spectral energy distribution fitting. It is forecast that the Wide Survey alone will contain over 60000 strong lenses, with the Deep and Ultra-Deep Surveys adding ∼2000 more.

In many cases, the CASTOR cosmology surveys will be further enhanced by the availability of red-optical and IR data from the Euclid[25] and Roman[26] missions.

4.2 Time Domain and Multi-Messenger Astronomy

Great efforts are being devoted to wide-field time-domain astronomy across the electromagnetic spectrum, as is apparent from the many ongoing and upcoming facilities, ranging from the optical (Rubin LSST)[23] to the infrared (Nancy Grace Roman)[30] and radio (SKA).[31] CASTOR can fill an important gap at UV wavelengths, particularly for the follow-up of transients. CASTOR has been designed to respond to external triggers within < 3 hours. Its simultaneous imaging in three bands (spanning $0.15 - 0.55$ μm) will allow rapid-assessment of the temperature evolution of hot and young transients with minimal ground-based support.

CASTOR will be a broadly valuable tool for time-domain astronomy, from explosive transients and exoplanets to moving objects and variable stars. In particular:

- *Explosive transients:* CASTOR will contribute to the study of explosive transients, including supernovae, peculiar and exotic transients, using two survey strategies: surveys with no pre-selection of targets, including CASTOR Cadence survey, and Target-of-Opportunity (ToO) observations in response to external triggers (see Table 3). Together these surveys will: (1) provide high-cadence UV light-curves for thousands of transients, supernovae and peculiar transients in their infancy; (2) deliver statistical samples of UV spectra for supernovae and more exotic transients like superluminous
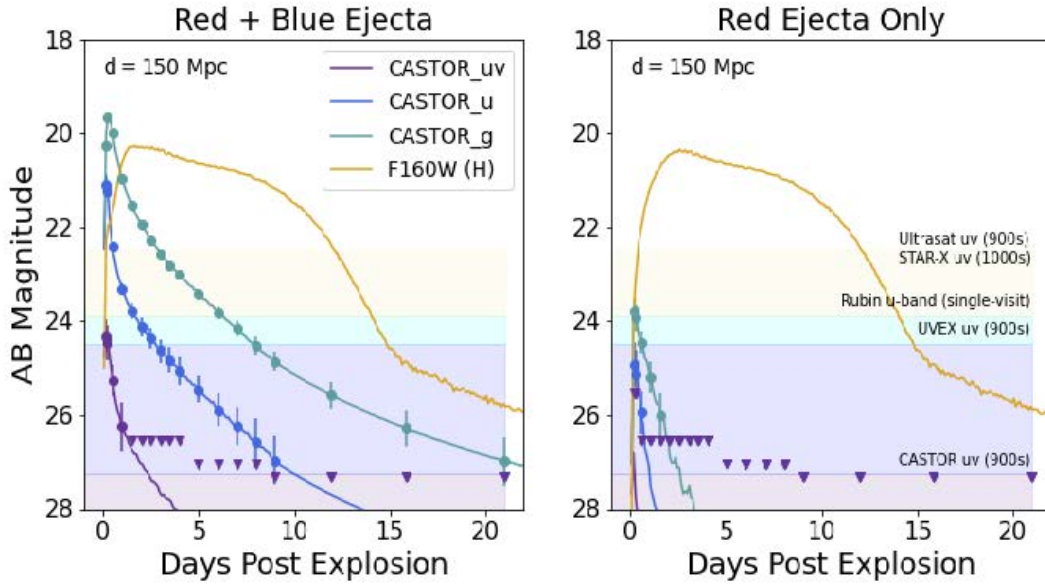
17

Fig 10 Mock CASTOR observations of a GW170817-like kilonovae at 150 Mpc using our baseline survey strategy described below. (Left). Expected observations for a transient with both a red (heavy r-process elements) and a blue (light r-process elements) ejecta component. (Right). Expected observations for a transient with only a red ejecta component. While the infrared emission (yellow curve) is almost unchanged, dramatic differences are evident in the ultraviolet and blue bands on a timescale of 1-10 days. Even at these moderate distances, tracing the evolution of the UV emission requires depths of $> 25 - 26$ mag AB. Quoted depths of various proposed UV/$u-$band survey missions are highlighted (with depth indicated at the upper boundary of each shaded region).

supernovae, tidal disruption events, and rapidly evolving transients; (3) perform rapid searches for EM counterparts of gravitational waves and neutrinos over large regions; and (4) facilitate studies of the local environments of extragalactic transients. Figure 10 shows CASTOR mock observations of GW170817-like kilonovae.[32]

• *Compact object binaries:* Close binaries containing compact objects (white dwarfs, neutron stars or black holes) are multi-messenger systems and represent the direct progenitors to compact objects mergers detectable by LIGO/Virgo/KAGRA and LISA. Multi-epoch photometric and spectroscopic surveys of the Galactic plane, star clusters, and the Magellanic Clouds will identify large samples of UV bright and variable objects, including detached white dwarfs, X-ray binaries, accreting white dwarfs, and stripped-envelope stars. Any such object's precise characterization can also be achieved with CASTOR's precision photometer, which will allow for the identification and characterization of tight white dwarf binaries (with periods < 30 minutes) needed as calibration standards for gravitational waves detection with LISA.[33]

Interacting binary systems hosting a compact object can undergo spectacular 'outbursts' lasting days to months, during which time they grow in mass and in radiative output by accretion of material from the companion star. In addition to the capability of tracking the long-term evolution of such outbursts, CASTOR's photometer will be sensitive to physically interesting sub-second timescales relevant for the inner accretion environments, with the simultaneous triple-channel coverage enabling new studies of the disk-jet interactions in such systems.[34,35]

• *Supermassive Black Holes:* CASTOR will study both active/accreting and quiescent black holes (SMBHs) through a dedicated reverberation mapping[36] campaign, measuring SMBH masses in thousands of galaxies out to redshift $z \sim 2.5$. CASTOR will also search for time-lag signatures indicative
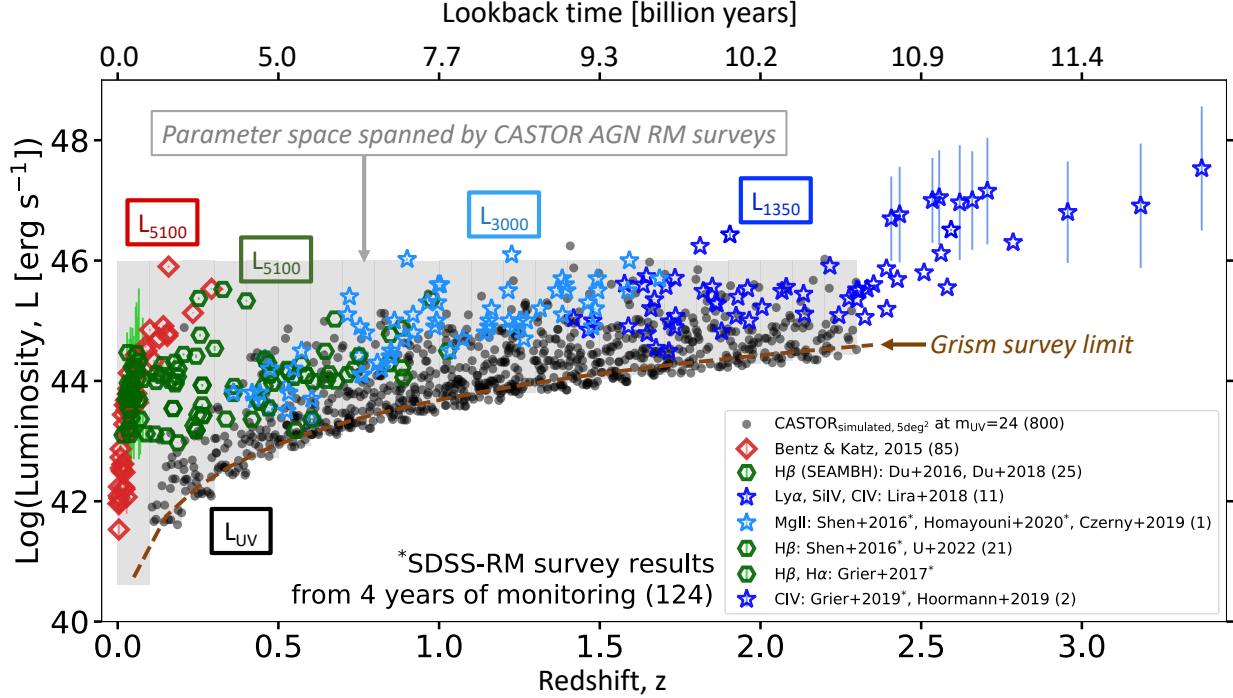
18

Fig 11 Luminosity-redshift parameter space spanned by CASTOR (light gray area) compared to all previous studies (colored symbols). CASTOR will be able to probe uniformly a unique region in the phase space of redshift and luminosity (black circles showing a simulated sample in 5 deg^2) as well as galaxy-host properties to study how black holes grow and how they affect galaxy evolution over 10 billion years of cosmic time.

of binary SMBHs[37] that will be detectable in gravitational waves from LISA and/or pulsar timing arrays, and mini-flares indicative of stellar mergers within AGN disks. Through its blind time domain surveys, CASTOR will also detect and localize hundreds of tidal disruption events, probing the extremes of the SMBH mass function.

4.3 Active Galactic Nuclei

At the centers of many, and perhaps all, massive galaxies lies a SMBH, typically with a mass of millions to billions of solar masses.[38] When SMBHs accrete gas from their surrounding environment, they release vast amounts of energy, with a profound impact on the galaxies in which they reside.[39] We call these rapidly-accreting SMBHs active galactic nuclei (AGN), yet we still do not understand how these objects grew to be so massive over cosmic time, nor their role in the evolution of galaxies.[40] SMBHs in the AGN state are relatively rare objects (with ~80 per deg^2 detected in soft X-rays),[41] with emission that peaks in the UV and varies over timescales of days to weeks or even years. Accurate measurement of the light from the central compact source requires a clean separation of the AGN from its host galaxy. CASTOR's unique sensitivity in the UV, large field of view, and high angular resolution make it a powerful tool for AGN imaging and spectroscopy.

Spectra of AGNs exhibit some prominent features at the short wavelengths to which CASTOR is uniquely sensitive: e.g., Ly-α, in emission and absorption, plus broad and narrow emission lines of NV, SiIV, CIV, HeII, CIII, MgII, [OII].[42] CASTOR will undertake a reverberation mapping (RM)[43] campaign that combines multi-band imaging and low-resolution slit-less UV spectroscopy over a region of 12.5 deg^2. By monitoring this field over a period of 4-6 months, CASTOR will measure masses for roughly a thousand

SMBHs — four times more than all previous AGN RM studies combined — over the largely unexplored redshift range $0 \leq z \leq 2.3$ (see Figure 11).

The Wide Survey will also detect AGNs at the centers of galaxies and resolve the associated star formation, surrounding ionized gas, and AGN jets. This will be possible for a vast number of galaxies spanning the last 4 billion years of comic history, sampling the full range in host environments from isolated galaxies to rich clusters. An exciting recent development in AGN physics has been the discovery of so-called "changing look" quasars, whose origin remains under debate.[44] Deep imaging from CASTOR, when combined with results from previous surveys, will make it possible to identify and study these rare systems. Finally, in the local universe, the relationship between nuclear star clusters and supermassive black holes in low- and intermediate-mass galaxies has emerged as an important question for galaxy evolution and feedback models, and CASTOR's UV imaging and spectroscopy will fill a critical niche in this area.

Synergies with current and future facilities will enhance the science return from all CASTOR AGN legacy and GO programs.[45,46] Red-optical and near-IR observations from LSST will further enable accretion-disk RM for a significantly large sample of $\sim$1000 AGN (probed by the AGN RM program). AGN campaigns with one or more of the next generation spectroscopic survey telescopes (e.g., the Maunakea Spectroscopic Explorer,[47] PFS/Subaru[48] or ESO's Wide-Field Spectroscopic Telescope[49]) will provide CIV black hole masses for high-redshift AGN, which will allow a consistent calibration of black hole masses over a vast range in redshifts.

4.4 Galaxies

Star formation, which drives the evolution of baryonic matter in the universe, acts as the primary regulator of galaxy evolution.[50] The evolution of star formation rate — both as a function of environment and over cosmic timescales — is thus central to our understanding of the physical mechanisms that drive, regulate and quench the evolution of galaxies.[51] UV radiation, which is usually dominated by short-lived, massive stars, provides our most direct probe of the star formation process.[52] However, distant galaxies are faint at UV wavelengths, and beyond the local universe, subtend only a few arcseconds on the sky. CASTOR's wide field of view, high sensitivity, and high angular resolution at UV/blue-optical wavelengths will open a new era in the study of cosmic star formation (see Figure 12).

With three nested imaging surveys — the Wide, Deep and Ultra Deep — the CASTOR sample will consist of tens of millions of galaxies spanning a huge range of masses and redshifts.[53] The Deep Survey (80 deg^2 to a 5σ per pixel surface brightness depth of $\sim$25.6 mag arcsec^{-2} in the UV) and the Ultra Deep Survey (1 deg^2 to $\sim$ 27 mag/arcsec^2) will provide extraordinarily sensitive imaging complementing CASTOR's Wide Survey. This will allow an unprecedented characterization of the evolution of the spatial distribution of star formation within galaxies out to redshifts of z$\sim$2.

In the local universe, the Nearby Galaxies Survey will carry out targeted imaging of $\sim$700 highly resolved galaxies, an unprecedented study of galactic star formation in the local Universe — especially in the low-density, outer regions that are effectively inaccessible to HST due to its much smaller field of view.

The grism instrument will provide a low-resolution spectrum for every object in CASTOR's field of view simultaneously, a powerful tool for detecting galaxies with strong emission lines or spectral breaks in the UV. Using CASTOR's grism mode, slit-less spectroscopy covering the 0.15 to 0.40 μm region will yield $\geq 10^5$ Ly-α emitters between $0.4 \leq z \leq 2.2$ in the Deep field, enabling a comprehensive map of the cosmic web. At the same time, Lyman continuum (LyC) detections for statistically complete samples of bright galaxies will offer an opportunity to characterize LyC emitters at "Cosmic Noon", when star formation in massive galaxies reached its peak.

In addition, the UVMOS observing mode will provide higher resolution spectroscopy, enabling the measurement of SMBH masses for AGN at $0.25 < z < 2.3$ (see §4.3) which is vital for understanding one of the primary mechanisms through which galaxies cease star formation over time.[40] Certain compact
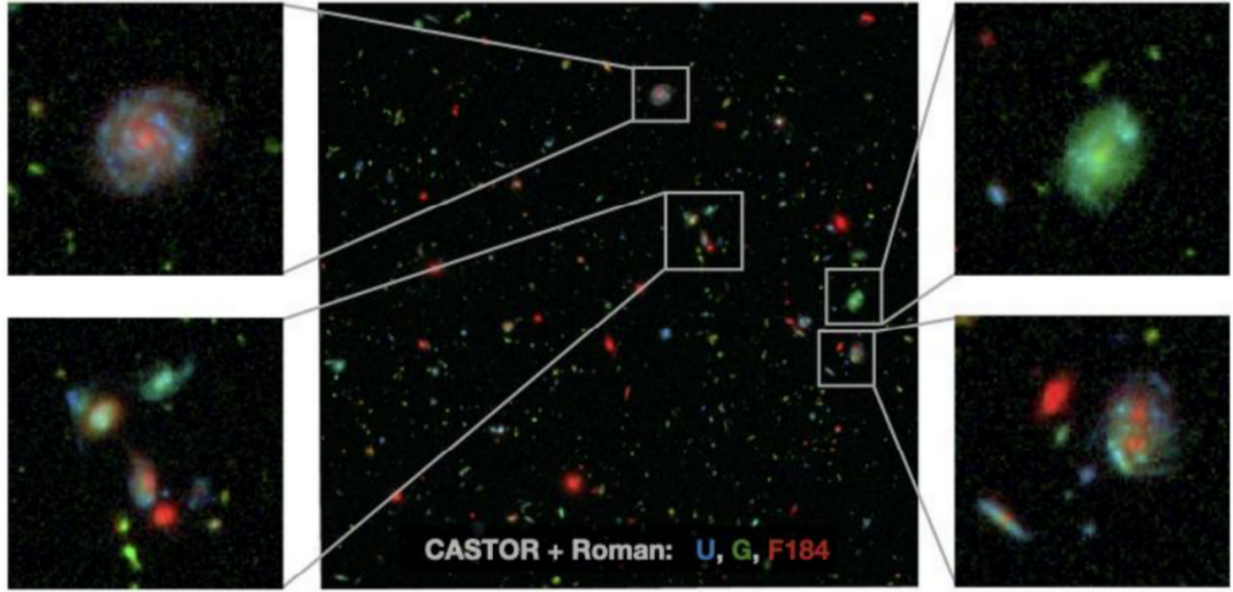
Fig 12 A simulation of part of the Hubble Ultra Deep Field (UDF) in passbands from CASTOR (u, g) and Roman (F184). This image shows a $\sim 1\overset{\prime}{.}5 \times 1\overset{\prime}{.}5$ field, or just $\sim 0.06\%$ of the area that will be covered by the proposed Ultra-Deep Survey. While Roman's IR imaging (red) is sensitive to existing stellar mass, CASTOR picks out regions of ongoing star formation. With comparable spatial resolution from the UV to the near-IR it will be possible to map stellar populations and other physical parameters across galaxies, out to cosmic noon.

extragalactic objects — such as Green Pea galaxies at $z \sim 0.3$ — would be ideal targets for the UVMOS instrument, which could resolve individual star forming regions with very low backgrounds. Taken together, legacy imaging and spectroscopic surveys will explore a range of galactic stellar masses over the past ~ 10 billion years of cosmic history, with a survey area sufficient to study some of the rarest galaxies in the Universe.

4.5 Near-Field Cosmology

Near-field cosmology aims to characterize the halo of the Milky Way and its substructures (satellite dwarf galaxies, globular clusters, stellar streams) in order to understand to what extent their observed properties are consistent with the predictions of cosmological models on sub-Galactic scales, in particular the cold dark matter (CDM) framework. CASTOR's dedicated imaging surveys will make multiple contributions to near-field cosmology:

- The CASTOR Galactic Substructures Survey will observe a representative sample of halo substructures (4 stellar streams, 57 globular star clusters, and 33 dwarf galaxies) in multiple bands, and with multiple epochs over the mission lifetime, in order to measure proper motions for stars fainter than the Gaia limit.[54] These observations will deliver clean samples of members for studying the morphology of these objects and for spectroscopic follow-up. Figure 13 shows, with mock data, how CASTOR will increase the number of streams identified and provide details of their morphology.

- The CASTOR Wide Survey will allow to study the metallicity distribution of the stellar halo and the most chemically pristine stars of the Milky Way.[55]

- The CASTOR Wide Survey, combined with Roman HLWAS,[56] will enable the discovery of new substructures in the Galactic halo, helping to assess the role of accretion events in its formation.

- With several key halo tracer populations uniquely characterized by CASTOR UV/blue-optical photometry (Blue Horizontal Branch BHB stars, blue stragglers, main-sequence turnoff stars), imaging programs like the Wide Survey will provide measurements of the density profile and virial radius of the Milky Way halo.[57] CASTOR will also make it possible to target halo tracers, such as BHBs, beyond our own Galaxy to probe the structure of Local Group galaxies like M31.
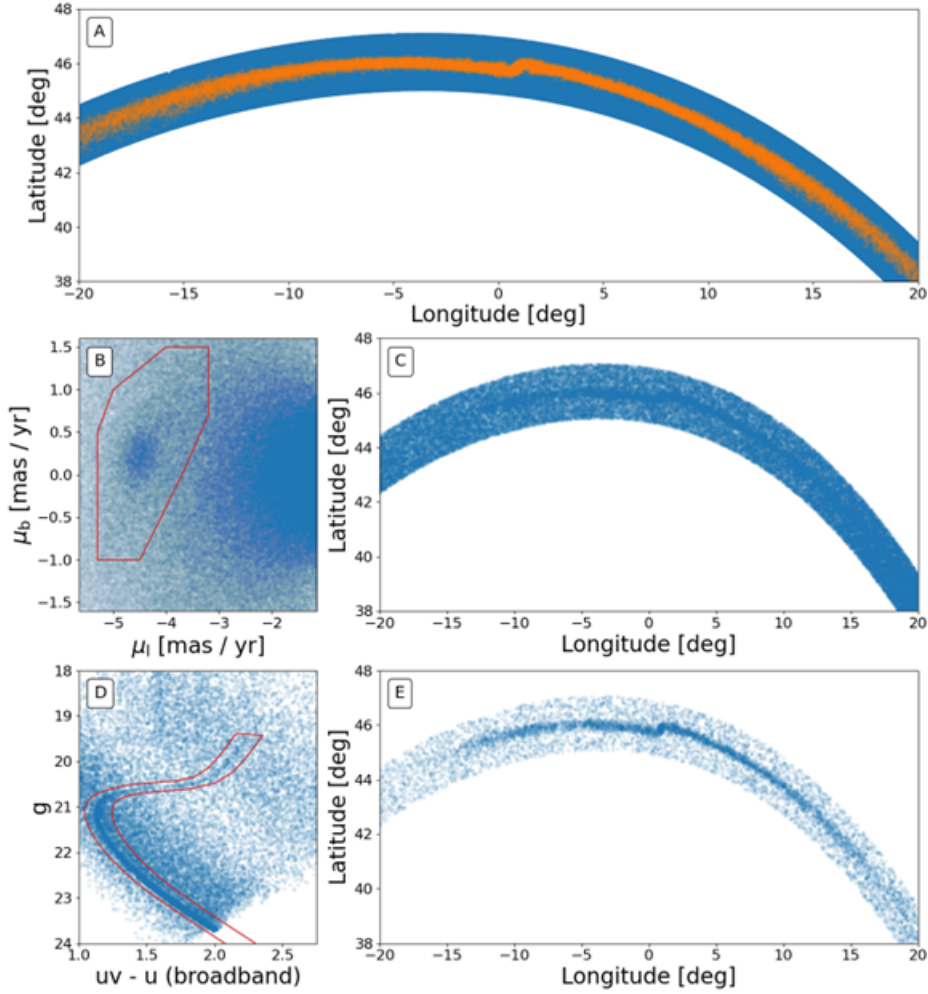

Fig 13 Mock CASTOR observations of the Pal 5 stellar stream (at a distance of 20 kpc) based on an N-body simulation of the stream (orange points in top panel) inside a smooth Milky Way halo (D. Erkal, private communication) combined with background/foreground contamination from Galaxia[58] stellar catalogues in fields surrounding the stream (blue points). On-sky positions of the stars are shown in the top and right panels. Panel C shows a selection based on the CASTOR proper motions (from panel B). A further selection based on the CASTOR colour-magnitude diagram (from panel D; along the metal-poor isochrone corresponding to the stream) is shown in panel E, where the stream appears as a clear overdensity. CASTOR's deeper observations (compared to Gaia) with a proper motion precision corresponding to 50 km/s or better at this distance (fainter stars with poorer proper motion precision are not included in this figure) will significantly increase the number of stream members identified, improve the contrast, and reveal an unprecedented view of stellar streams and their morphology.

CASTOR spectroscopy would also enable a range of near-field cosmology programs: e.g.,

- Using the UVMOS instrument, it will be possible to measure the chemical makeup of stars in globular cluster cores, generally too crowded for ground-based spectroscopy.[59]

- Through GO programs, CASTOR slit-less spectroscopy could be used to trace stars bearing the chemical signature of multiple populations across stellar streams and constrain the nature of the progenitors of these streams.[60]

- Slit-less UV spectroscopy from the Square Kilodegree Galactic Plane Survey and the Grism Legacy Survey will enable serendipitous discoveries of chemically peculiar stars and extremely metal-poor stars in the Galactic halo and bulge.[61] Slit-less UV spectroscopy would be valuable for probing the mix of stellar populations in compact stellar systems around nearby galaxies and in nearby clusters.

4.6 Stellar Astrophysics

The UV region has a special importance in stellar astronomy. Unobservable from the ground, this region is highly sensitive to hot continuum sources, such as the high-mass stars that are disproportionately responsible for the synthesis, ionization, and dissociation of elements, as well as the kinetic energy input to galaxies.[62] The UV region also harbours a wealth of atomic and molecular spectral features, including numerous resonance transitions, while the UV continuum is highly sensitive to the integrated light of young stellar populations, making it a powerful diagnostic of recent star formation.[52]

CASTOR's imaging capabilities will be uniquely suited to UV/blue-optical studies of stellar objects. The Square Kilodegree Galactic Plane Survey will image the galactic plane and bulge over $\sim$1100 deg^2 in three passbands, detecting hundreds of millions of stars with a depth of 25.5 AB mag, and revealing thousands of the hottest massive stars (Wolf-Rayet and OB supergiants). The Wide Survey will itself observe half a million white dwarfs, with the UV/u/g filters able to effectively separate standard hydrogen-atmosphere white dwarfs from more exotic objects, including double white dwarf merger products and white dwarfs that are accreting rocky planetary material.

CASTOR's imaging and spectroscopic capabilities are also well suited for monitoring the flaring properties of M stars. A dedicated monitoring campaign will measure the M star flare rates across stellar ages and masses, assessing the habitability of the 40 billion habitable zone terrestrial exoplanets orbiting M stars in our galaxy. Similarly, observations in the UV band will permit the monitoring of the accretion variability of young protostars.
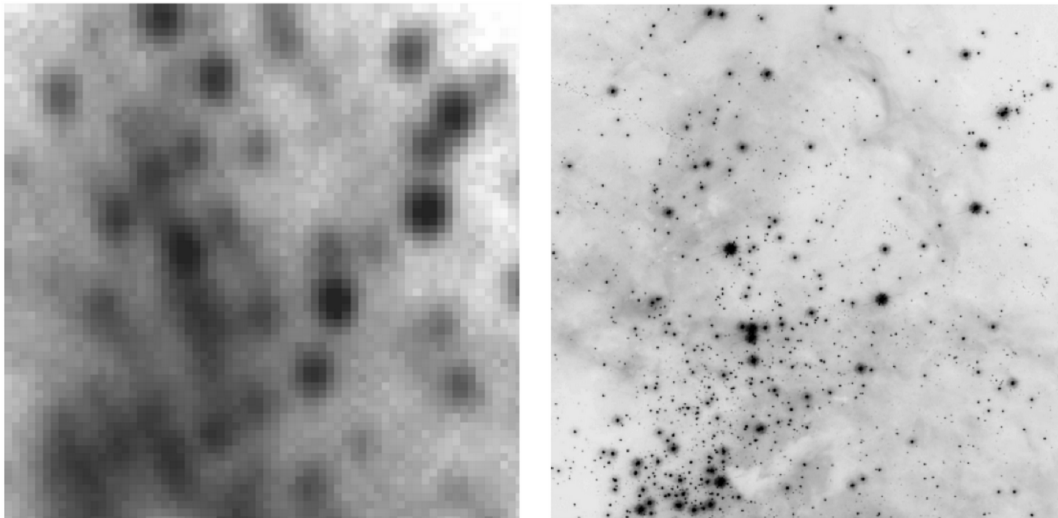

Fig 14 Observations of a $100''\times100''$ region in 30 Doradus from GALEX/NUV (left) and simulated CASTOR observations (right) based on smoothed data from HST/WFC3 F275W. The depth is 24 mag, so the CASTOR Magellanic Clouds survey will reach about 50 times deeper.

The Magellanic Clouds imaging survey will provide a database for the study of massive stars, clusters, accreting compact objects, and supernova remnants in a low-metallicity environment markedly different than that of the solar neighborhood (Figure 14).[63] CASTOR imaging surveys will discover previously missed supernova remnants, planetary wind nebulae and neutron stars in the Milky Way and Magellanic Clouds. CASTOR's angular resolution and sensitivity will allow the detection of white dwarfs in clusters within the Magellanic Clouds. These observations will provide much-needed constraints on the initial-final mass relation of stars. Repeated imaging over multi-year baselines will allow precise proper motion measurements, enabling clean samples of cluster members for populations that are beyond the magnitude limits of Gaia.

In addition to the science cases enabled by CASTOR's imaging capabilities, its spectroscopic observing modes will further enable revolutionary stellar astrophysics. CASTOR's UVMOS will be able to characterize the chemical makeup of stars in globular cluster cores, where severe crowding makes ground-based spectroscopy impossible. Several programs are planned to serve this need using CASTOR's UVMOS, targeting massive star populations in the Carina Nebula, Tarantula Nebula, and others. Finally, grism spectra taken in the Galactic Plane Survey will enable a study of galactic reddening law variations in synergy with the Roman Galactic Plane Survey,[30] providing a probe of the extinction due to interstellar dust.

4.7 Exoplanets

Evidence from direct imaging studies, transit surveys, and radial velocity monitoring campaigns has revealed exoplanetary systems to be commonplace. The physical properties of known exoplanets — such as their masses, radii and orbits — are surprisingly diverse and include classes of objects without analogs in our solar systems: e.g., "super Earths" and "mini-Neptunes". Exoplanetary systems provide direct insight into how Earth-like planets capable of sustaining life may arise.

CASTOR will be able to leverage its 1m aperture and UV/blue-optical sensitivity to obtain high-precision photometry and low-resolution spectroscopy of exoplanets and their host stars. The CASTOR passbands are unique among any operational astronomical spacecraft, including JWST, except for the aging HST. These wavelengths provide a unique window into the structure and composition of planetary atmospheres through Rayleigh scattering and molecular absorption. With optimized CMOS detectors in each of its three focal planes, and wide-field imaging capabilities that will enable photometric monitoring surveys in crowded fields, CASTOR's legacy surveys and GO programs can address several questions in exoplanet research:

- *Transit spectroscopy*. Transit surveys of bright transiting exoplanet systems will be used to measure atmospheric scale heights and scattering properties, providing information on how atmospheres survive and evolve. Such measurements are essential for interpreting measurements made at optical and IR wavelengths since UV-blue observations sample the Rayleigh slope, making it possible to establish the presence of scattering hazes and cloud decks in the upper atmospheres. By targeting the UV/blue-optical region, CASTOR will complement observations at red-optical/IR wavelengths from JWST, TESS, ARIEL and PLATO to separate exoplanet transit signatures from star spot artifacts.

- *Exoplanet albedos*. The sensitivity of CASTOR will enable high-precision phase curve measurements for exoplanets orbiting bright stars (i.e., planets ranging from Jupiter to Earth sizes will be accessible). Phase-curves provide unique measurements of scattering angles to reconstruct particle size distributions, cloud properties and potentially even meteorological studies.

- *Kepler habitable zone planets*. Follow-up multi-wavelength transit measurements for candidate Earth-sized exoplanets in the habitable zones of Sun-like stars will allow candidate validation and the elimination of false-alarms from the Kepler habitable zone sample. Such data can yield true "eta-Earth" measurements to enable validation.

- *Exoplanets in Globular Clusters and the Galactic bulge.* In its wide-field imaging mode, transit surveys in the UV, u, and $g-$bands that target dense star fields (i.e., bulge fields or globular clusters) can provide a window into the number and properties of exoplanets in new, or under-explored, environments or metallicity/age regimes.[64,65]

- *Bulk composition of rocky material in white dwarfs.* UV/blue-optical imaging and low-resolution spectroscopy from CASTOR (such as that from the Wide, Deep, Cadence or Grism surveys) will make it possible to efficiently identify and derive abundances (Mg, Fe and Ca) for thousands of metal-polluted white dwarfs, which have accreted heavy materials from planetesimals, asteroids, small planets and comets.[66,67]

4.8 Solar System

Small bodies in the solar system — such as near-Earth objects, asteroids, comets, trans-Neptunian objects (TNOs)[68,69] and members of the distant Oort cloud[70,71] — are debris that failed to coalesce during the formation of the major planets. The study of these bodies opens a window to the dynamics of the forming solar system, the chemistry of the primordial planetary disk, the densities within that disk, and the process of planet formation. By taking into account the properties of these bodies in the comparison between exo-disks observations and exo-planetary systems, we can explore planetary system similarities, conditions for life, and our planet's place in the Galaxy.
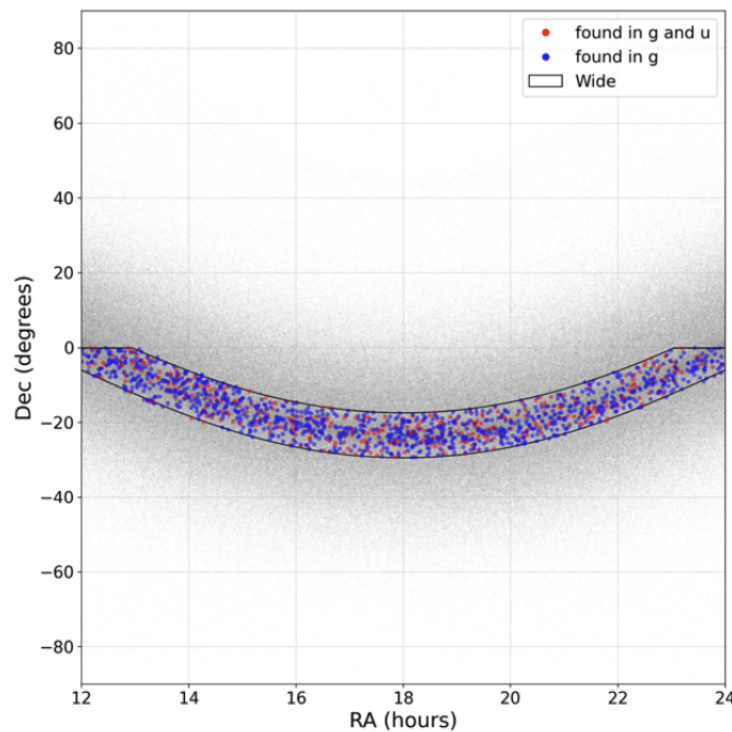

Fig 15 Simulations of the TNO wide survey component from a high precision model of the outer Solar System.[72] The wide footprint will include all objects within $6°$ of the ecliptic and having $\delta < 0°$, the region that will be best sampled by LSST. Colored points show the objects detected by the wide component of the CASTOR census of TNOs. Red symbols show objects are detected in both u and g; blue symbols show objects detected in g only. For clarity, the figure shows only 10% of total model and detected objects and only the 12h-24h zone, the part of the ecliptic south of the equatorial plane.

CASTOR has several unique capabilities for exploring these small bodies. Three strategic surveys,

designed to explore the present-day properties of the minor planets in our solar system, will probe the process of planetesimal formation:

- The Faint component of a TNO survey will reach smaller sizes than any existing or planned ground-based project while searching a significantly larger area of the sky than is feasible from JWST. Such programs provide a tie-in between the very faint and small KBOs (Kuiper Belt Objects) that JWST will probe and the much larger objects that can be studied from the ground.

- The Wide component of a TNO survey will measure u-band surface colours of all KBOs that LSST will detect in the southern sky. The LSST southern survey will provide a large sample of KBOs with well-measured orbits and optical surface properties. With CASTOR, we can extend that coverage into the u band where the silicates on the KBOs surface dominate the spectral reflectance, probing the chemistry of the disk at the time of planetesimal formation. Figure 15 shows simulations of the CASTOR wide survey in the g and u bands.

- The third component of the survey will utilize CASTOR's grism capability to undertake a survey of spectral reflectance of KBO surface properties. The grism spectra will probe the spectral features whose bulk properties will be probed by the wide-area u-band survey of LSST-discovered southern KBOs.
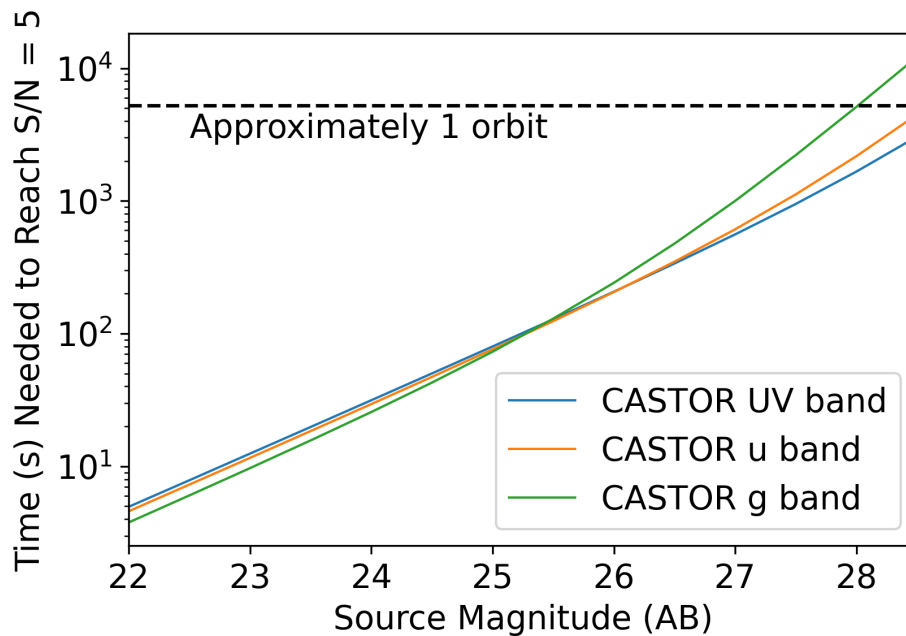

Fig 16 Point-source sensitivity (AB mag) in each of CASTOR's three primary passbands, expressed as the time needed to reach a signal-to-noise ratio of S/N = 5. The time for CASTOR to complete a single orbit is shown as the dashed horizontal line.

5 Current Development Activities

As noted in §1, the mission team hopes to begin a Phase A study in 2025. During that development phase, the system conceptual design, system requirements, concept of operations, and operations requirements will be further advanced while simultaneously raising the TRL of critical technologies and mission elements. A number of development efforts are already underway, and we present brief descriptions of these below.

Given the CASTOR design, these programs are heavily focused on UV and blue-optical technologies and so are relevant to the HWO mission which is aiming to begin operations in the 2040s. Ongoing or planned future activities for CASTOR include the development and testing of UV-enhanced CMOS arrays; light-weighted, low-expansion mirrors in the UV; polished optics with smoothness and micro-roughness requirements appropriate for UV wavelengths; UV multi-shutter systems; and high-performance, stable dichroics, grisms, gratings, and mirror coatings for use in the UV. As an example, an updated design study for the dichroic coatings is now underway at the UK-Astronomy Technology Centre (UKATC), with support from the UKSA. This program aims to maximize throughput in the UV, better define the photometric passbands, and minimize red leak in the UV channel.

The CASTOR science program, which will focus on survey and pointed observations at UV/optical wavelengths — during a time frame roughly bracketed by the probable end of HST operations and the launch of HWO — will itself help define a scientific pathway to the beginning of the HWO era.

5.1 Science Planning Tools

The design, development and implementation of CASTOR's instrumentation and science surveys requires a unified software framework for mission and survey planning, as well as supporting future GO proposals. To this end, the University of Manitoba, in partnership with NRC's Herzberg Astronomy and Astrophysics Research Centre (NRC-HAA), is leading the development of "Finding Optics Requirements and Exposure times for CASTOR" (FORECASTOR), a suite of simulations of CASTOR's full optical chain, survey strategy, and anticipated science results. The FORECASTOR tools are developed under three guiding principles:

1. The code base, as well as all simulation input data and results, should be open source and accessible through multiple channels, to enable a wide and diverse contributor and user base, and in keeping with the Government of Canada's Open Data policy framework.

2. To the greatest possible extent, the tools should be written in the Python programming language, for ease of use within the astronomical community and to maximize interoperability with existing, publicly-available astronomy software.

3. All tools should be available and executable within Jupyter Notebooks on the Canadian Astronomy Data Centre (CADC)'s Canadian Advanced Network for Astronomy Research (CANFAR) platform[73,74] so that any individual or team can both utilize and contribute to the development of the FORECASTOR tools independent of their local resources, on a shared, integrated platform.

The first tool released within this framework is the FORECASTOR Photometry Exposure Time Calculator (CASTOR_ETC),[17] a Python package that allows the user to carry out signal-to-noise calculations for CASTOR or other instruments (see, e.g., Figures 16 and 17). In addition to a suite of Python modules and associated Jupyter Notebook templates, a graphical user interface was also developed for the CASTOR imaging and photometry ETC (§2.4.1), available through the CADC CANFAR platform. A specific tool for exoplanet studies (§4.7) using the planned precision photometer instrument (§2.4.2) has also been released within the same graphical interface, developed in collaboration with the Photometric Observations of Exoplanet Transits (POET) team.[75] A preliminary exposure time calculator for the DMD-based UVMOS instrument (§5.4) was developed within the same pixel-based, user-friendly framework as the imaging and photometry ETC, and incorporated into the same workflow (with the addition of a "UVMOS" Object).[76]

An exposure time calculator and full scene simulator for the grism mode (§2.4.1) has been developed and a beta version is publicly available.[3] The tool has been primarily developed and tested for planning of the Grism Legacy Survey (see §4.4). Figure 18 shows the simulated CASTOR grism spectrum, in the
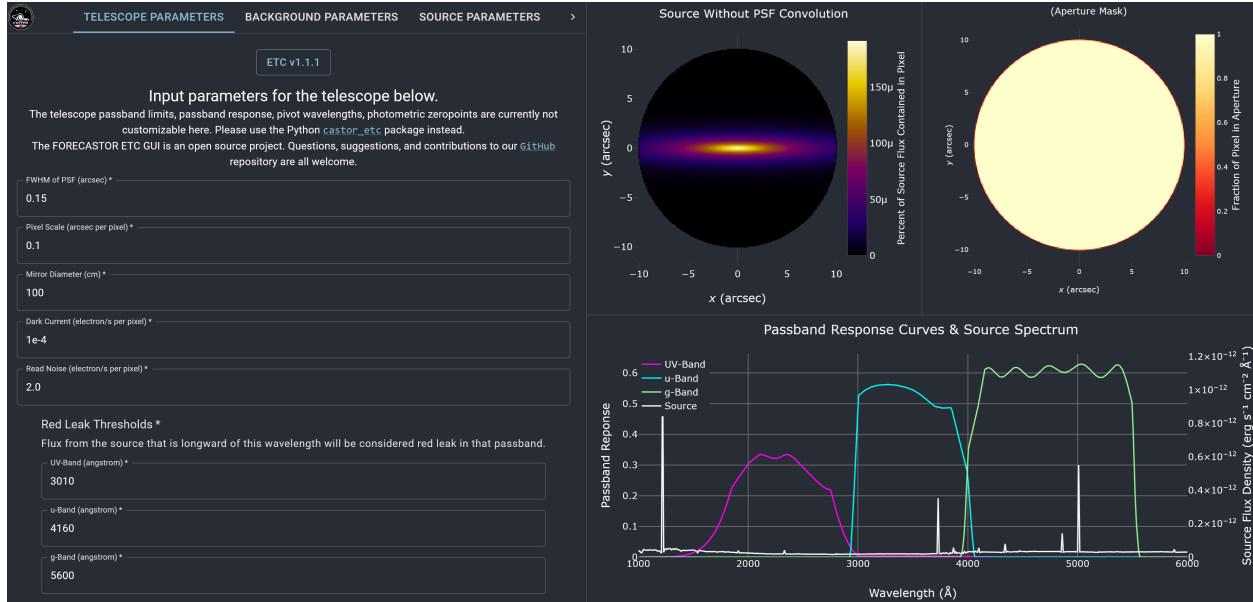
---

[3]https://github.com/gnoir0t/ETC_grism

Fig 17 Sample screenshot from the web application developed for the FORECASTOR suite on the CANFAR Science Platform.[17]

u-channel, of a $u = 23.4$ mag (AB) Lyman-break galaxy at $z = 2.793$, after six hours of exposure. As the time of writing (v0.7.0), the tool also offers simulating full grism scenes with overlapping sources and spectra, as well as redshift fitting of grism spectra for extragalactic sources (Noirot et al., in prep). A lite version of the grism ETC for single sources is incorporated in the FORECASTOR GUI presently available on CANFAR.

To simulate realistic images for CASTOR's planned field surveys of galaxies (Figure 19), FORECAS-TOR employs an adapted version of the open-source Python package GALSIM.[79] For our baseline predictions for the Wide, Deep, and Ultra-Deep surveys,[53] we draw expected galaxy populations from the "Santa Cruz" semi-analytic model-derived catalogue[77,78] to provide model CASTOR band magnitudes for hundreds of millions of galaxies spanning 10 billion years of cosmic history. Simulations of resolved stellar populations can also now be carried out using a modified form of the publicly-available ArtPop Python package.[80] ArtPop takes synthetic photometry in a given passband, together with input properties of a given stellar system and a chosen observing facility, to produce output images with realistic modeling of the instrument performance included. A Python wrapper for ArtPop, also available as a Jupyter Notebook, has been developed which includes CASTOR UV, u, and g passbands as well as the u and UV channels when divided by the deployable broadband filter (see Figure 2 and §2.4.1).

Additional software development for the CASTOR mission continues with the support of NRC-HAA. This includes support for the UVMOS instrument (see § 5.4), as well as a survey scheduler and optimization tool developed in partnership with Magellan Aerospace. Detailed simulations of the performance of the CIS300 series of detectors, given the expected specifications and environment of CASTOR, are presently being developed using the Pyxel python package,[81] in collaboration with the University of Manitoba and with the support of the Open University and the UK Space Agency. In addition to being available on the CADC's CANFAR Science platform, all FORECASTOR tools are published on https://github.com/castor-telescope as soon as they are prepared for public release.

Pre-Phase A science development for the mission is also underway with support from the UKSA through its Science and Exploration Bilateral Programme. Several of the science planning tools described above are being refined and applied through this effort, which focuses primarily on science applications in areas of near-field cosmology, galaxy evolution, TDAMM science and the solar system. This work involves a collaboration between the University of Edinburgh's Wide Field Astronomy Unit (WFAU) and the Canadian
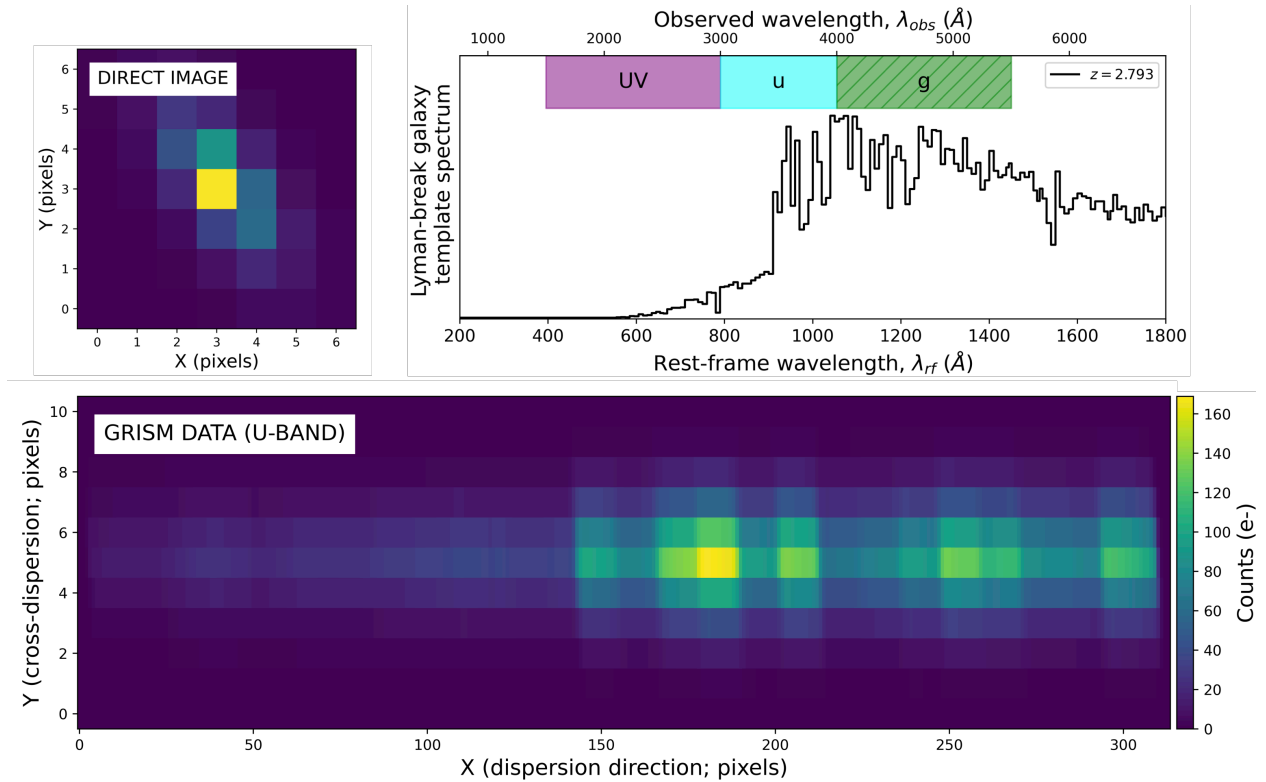
Fig 18 Simulated CASTOR grism spectrum of a Lyman-break galaxy at $z = 2.793$. The top left panel shows the simulated direct image of the source ($r_{\rm eff} = 0.15''$, ellipticity of 0.55, Sérsic index $n = 1.05$) at CASTOR resolution. The top right panel shows the Lyman-break template used for the source SED. The shaded bands show the wavelength range of the CASTOR UV, u, and g channels (purple, cyan, and hatched green, respectively). Only the UV and u channels have grism capabilities. The bottom panel shows the noiseless electron counts of the simulated grism spectrum after 6 hr of exposure for a $u = 23.4$ mag (AB) source. The grism tool also simulates the noise properties of the grism observations (including the sky background, read noise and dark current) to produce SNR maps and derive exposure times.

Fig 19 Simulated images for a small patch of CASTOR's planned Wide Survey in the UV, u, and g channels, generated using a synthetic light-cone catalog drawn from published semi-analytic models of galaxy populations.[77,78] With total exposure times in the range 1000–2000 sec, these images reach 5σ point-source depths of ~ 27.5 in all three channels.

Astronomy Data Centre (CADC) to define CASTOR data flow system including the definition of requirements for a CASTOR alert broker.

5.2 Vacuum Ultraviolet Calibration Facility

Mission development is making use of the Vacuum Ultra-Violet Laboratory (VUVLab) located at the University of Calgary (Figure 20). This is a specialized facility designed for the testing of photosensitive detectors that operate at UV wavelengths. The VUVLab was previously used to characterize the UV-sensitive photon-counting CMOS devices used in the Ultra-Violet Imaging Telescope (UVIT) on the Astrosat mission[13,82,83] that was led by the Indian Space Research Organization. The VUVLab is now being repurposed for the testing and characterization of new CIS120 CMOS sensors, variants of the devices slated to fly aboard CASTOR.

The facility consists of a clean room, within which sits a 0.544 m^3 stainless steel vacuum vessel connected to separate optical and UV arms. The latter arm contains an ARC Model DS-775-100 Focused Deuterium Light Source and adjoining Model VM-503 monochromator assembly capable of producing a broad-spectrum 115 nm $\lesssim \lambda \lesssim$ 370 nm UV emission, with multiple distinct emission lines below 165 nm. Rays are collimated and attenuated through an aperture assembly before passing into the main vacuum chamber, where an engineering grade CIS120 detector can be mounted together with an LN2-mediated temperature control system on a five-axis manipulator assembly. The manipulator is capable of three translational degrees of freedom, as well as two rotational, which allows for a comprehensive coverage of the detector. LN2 cooling lines and readout electronics are provided via feed-throughs to permit the entire volume of the vessel to be held at a consistent vacuum. The LN2 passes through a copper heat exchanger block which, in tandem with a temperature control and heater unit, keeps the sensor at the operating temperature. Lastly, a NIST-calibrated photodiode will soon be installed to provide an accurate measurement of the UV flux entering the test chamber.
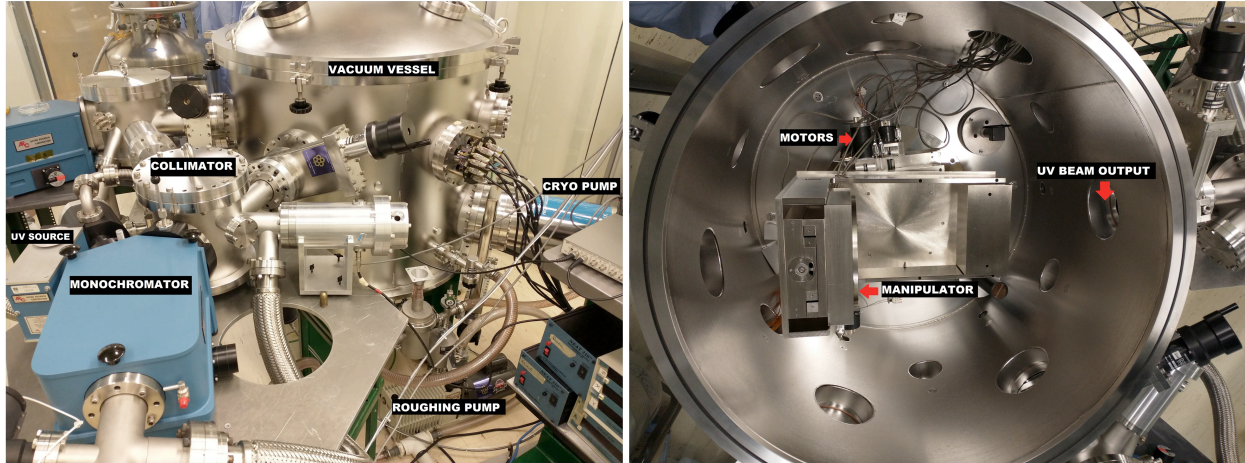
Fig 20 (*Left*) View of the exterior hardware. (*Right*) Manipulator mounted inside of the vacuum vessel.

The vacuum itself is achieved through a two-stage pump down. Initial pumping from atmospheric pressure is achieved by two Varian SD-450 roughing pumps, and the second stage from $\sim 10^{-3}$ torr is handled by a water-cooled cryo-pump that allows trace gases to condense upon a cold surface. Vacuum pressure is monitored initially via thermocouple gauges until pressure is low enough that Bayard-Alpert (ionization) gauges take over below $\sim 10^{-4}$ torr. In anticipation of renewed testing in the VUVLab, the vacuum capability of the setup was verified upon light refurbishing of the equipment including new oil mist eliminators and coaxial traps. Furthermore, the cryo-pump and pressure gauges were tested to ensure their integrity. Presently, the system is capable of achieving pressure stability of $10^{-(7-8)}$ torr within 24 hours of initial pump down.

To mount the CIS120 device and temperature control system to the manipulator assembly, a custom interface was designed and fabricated. The mounting system is composed of stainless steel, aluminum, and G10 composite that together provide a secure mounting system for the detector, LN2-cooled Cu cooling block, and calibration diode with excellent thermal stability properties. The 5-axis manipulator provides fine control of the sensor orientation with respect to a collimated UV beam, with a minimum precision on the order of sub-millimeter translation and hundredth of a degree in rotation. Control is achieved via stepper motors feeding data to display units constructed in-house.

The ongoing work aims to provide as complete a characterization of the CIS120's imaging performance as possible, by conducting measurements of dark current and quantum efficiency over the full range of expected temperature conditions. The standard set of astronomical calibration frames will be collected (darks, biases, and flats), to which end an integrating sphere will be employed in order to provide an even illumination across the full sensor area. Furthermore, all tests imaging capability will be conducted over a range covering the near (370 nm) to far UV (115 nm).

5.3 Detector Testing and Calibration Programs

Despite its modest 1m aperture, CASTOR will rival the sensitivity of the 2.4m HST largely due to advances in UV detectors. The baseline imaging detector for the CASTOR mission is the Teledyne-e2v CIS300 series CMOS device, currently under development at Teledyne-e2v. This detector has both low dark current ($\lesssim 0.01\ e^-\ \mathrm{px}^{-1}\ \mathrm{s}^{-1}$) and read noise ($\lesssim 6\ e^-$ rms). A CSA-funded STDP study, which advanced mission readiness, included a work package for the advancement of detector technology. This effort included TRL advancement for the detector FPA and ongoing development of the delta-doping process on CIS series Teledyne-e2v detectors. As part of this STDP study, a mechanical prototype of the FPA was designed, built

31

and used to demonstrate that critical flatness requirements can be maintained both over the SCA and the FPA after assembly.
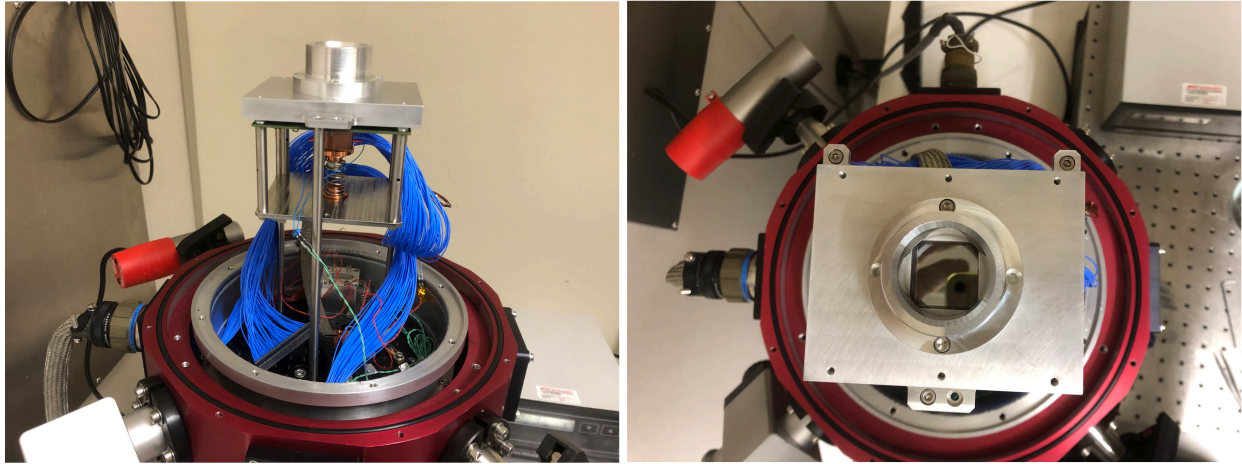

Fig 21 Two views of the CIS120 detector and platen installed in the cryostat at NRC-HAA.

Delta doping is a surface passivation process for silicon detectors developed by JPL. This process alleviates the problem of charge trapping of photo-electrons in silicon detectors. UV detectors are particularly prone to charge trapping due to the shallow absorption depth of the UV photons. The JPL delta doping technique is unique in that, by using low-temperature molecular beam epitaxy, the surface doping can be controlled to near atomic-scale precision. Being a low-temperature process, it can also be used on fully-fabricated devices. With this process, 100% internal quantum efficiency (QE) has been demonstrated, meaning that the QE of these devices becomes a reflection limited response. JPL has also advanced antireflective coating on silicon detectors using atomic layer deposition to maximize in-band QE.[84, 85]

A UV-enhanced CIS120 prototype is being created under a cooperative development program between the CSA and JPL, and working with Teledyne-e2v. In 2023, a set of CIS120 detectors were delta doped and antireflection-coated for enhanced UV sensitivity. The performance of these detectors is now being quantified in an international effort involving NRC-HAA, the University of Calgary, and the Open University (UK). The Open University is currently testing the detectors down to 150 nm in their UV detector test system. NRC-HAA is working with the University of Calgary to independently test the detectors down to 150 nm using the VUVLab in Calgary (see §5.2 and Figure 21). NRC-HAA has recently completed a CIS120 readout electronic system that will allow the detectors to be controlled in the VUVLab test chamber. Initial testing is focusing on detector read noise, dark current as a function of temperature, device uniformity and quantum efficiency. Upcoming tests will include out-of-band QE, image persistence, and read noise versus clocking speed and temperature. An upgrade to the test system which will allow the imaging of a PSF on the detector for characterization of intrapixel capacitance and charge diffusion is in development.

A complementary effort to develop, test and characterize the CASTOR detectors is underway in the UK with support from the UKSA. The Open University is undertaking the first steps to test and space qualify T-e2v CMOS devices for the precision photometer (CIS120/220) as well as for the imager and spectrograph (see Figure 22).[86] A significant part of this program is a contribution from T-e2v to accelerate the development of the radiation-hardened CIS 300-series detectors to align with the CASTOR timeline. A comprehensive radiation testing campaign is being planned, which will include total ionizing dose (TID), total non-ionising dose (TNID) and single event testing. The program aims to raise the TRL level to 5/6, as well as de-risk the performance and manufacturability of the UV enhancement technologies used for the detectors. Using CIS120 devices, three different coating technologies will be tested: 2D-doping (JPL); black silicon (Aalto Uni/Elfys); and UV enhanced coating (T-e2v). Work is also underway to model the CASTOR
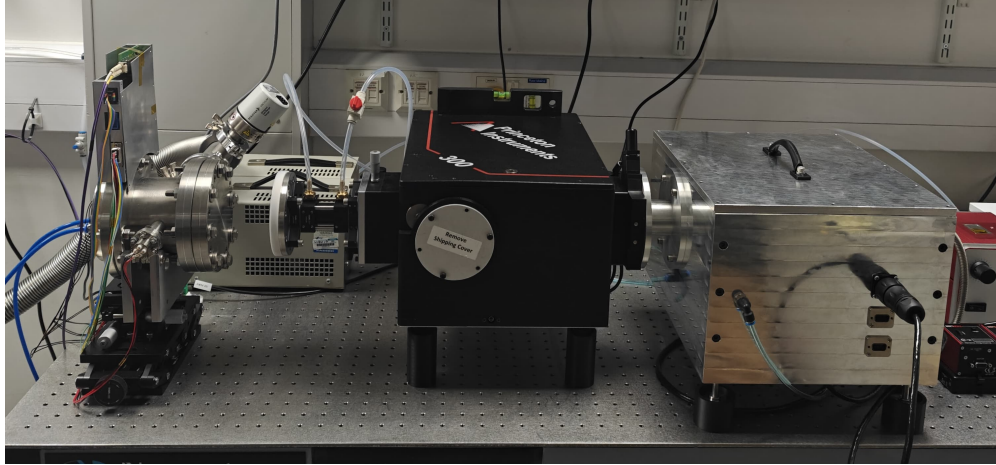
Fig 22 CIS120 and monochromator test setup at The Open University. A CIS120 device is mounted inside the vacuum chamber on the left, currently set up for dark tests. The chamber on the right is a housing for a dual deuterium and halogen lamp feeding the monochromator in the middle.

radiation environment and assess the radiation backgrounds that will be experienced by the instruments and payload. The results of modeling will be used to determine the local shielding design needed for in-orbit protection. In a related effort, the University of Leicester is now commissioning a vacuum-UV test facility for the calibration of the CASTOR sensor, and developing a top-level electrical, mechanical and thermal design for the front-end electronics.

5.4 UV Multi-Object Spectrograph: Design and Prototyping

A medium-resolution, multi-object spectroscopic capability was identified as a scientifically interesting capability during the 2019 CASTOR science maturation study. A UVMOS instrument would enable compelling scientific investigations in its own right, and ensure a flexible UV spectroscopy capability in the post-HST era. It is possible that HWO will feature a MOS capability in the UV/optical region, so UVMOS development for CASTOR will raise the technology readiness level of instrument designs that feature a digital micro-mirror device (DMDs) as the object selector.

The CASTOR UVMOS is based on that of the BATMAN spectrometer[87] which was designed for use at optical wavelengths and successfully tested on ground-based telescopes.[88] The optical design is an Offner-type system (Figure 23). The Offner *relay* is an elegant optical system consisting of three spherical mirrors configured symmetrically about the stop; this symmetry cancels the Seidel aberrations to provide high-quality imaging. An Offner *spectrograph* is a modified Offner relay with the convex mirror replaced with a grating. This design is ideal for UV optics since it incorporates all reflecting optics — avoiding the UV absorption that is inevitable in lenses — with only three reflections in a compact system. The multi-object slit is a modified TI DLP9500 DMD. The DPL9500 has an array of 1920×1080 10.8 μm pitch MEMS micro-mirrors. Each micro-mirror measures $0.^{\prime\prime}108$ on the sky and can be independently switched between two states for object selection.

The CASTOR UVMOS design employs a DMD, as opposed to a microshutter array, for several reasons. Most crucially, the physical size of DMD micromirrors (10.8 μm for the DLP9500) and high fill factor are better matched for CASTOR's image scale, than the much larger microshutters (100×200 μm), which would result in spatial sampling of $1^{\prime\prime} \times 2^{\prime\prime}$ on the sky. Furthermore, although the Next Generation Microshutter Arrays[89] (NGMSAs) currently in development by NASA represent a significant improvement over the magnetically actuated arrays developed for JWST, the NGMSAs still show significant rates of inoperable shutters.[90]

On the other hand, DMDs that are being actively developed for astronomical applications in the UV and the CASTOR UVMOS design faces three challenges of its own:
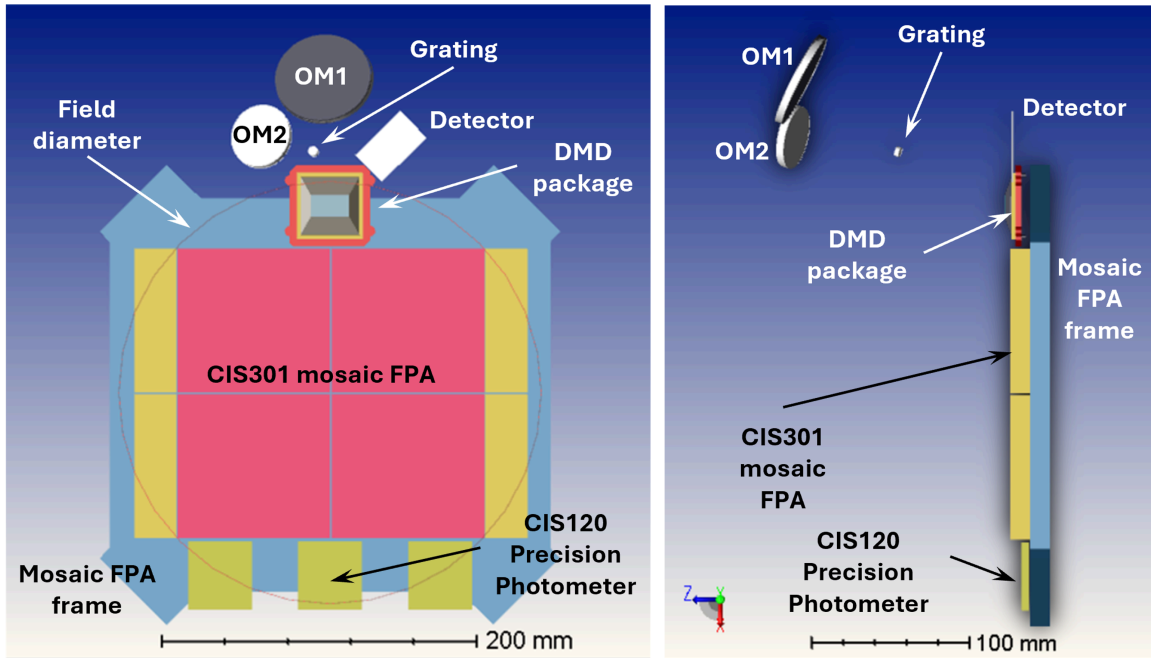

Fig 23 Front and side view of the UVMOS optomechanical concept. OM1 and OM2 refer to the first and second Offner mirrors.

1. **UV performance of DMDs**: While such devices have been thoroughly studied (and mass-produced) for operation at visible wavelengths, additional development is needed for use in at UV wavelengths and in space environments.[91,92]

2. **Convex UV gratings**: The use of a convex grating enables an efficient and compact design, an important consideration for space missions. However, development is needed to produce a UV grating with high efficiency, low wavefront error, and low scattering for use in the UV region.[93]

3. **UV detectors**: CMOS devices were selected as the baseline detector for the mission following a careful performance ranking of competing technologies. Further advancement in characterizing these state-of-the-art detectors is required to mature this exciting technology, including the delta-doping processes that will be used to maximize their quantum efficiency at UV/blue wavelengths (see §5.3).

In spring 2024, NRC funded, through its "Small Teams" program, a three-year project to mature these three technologies. The study is now underway, led by NRC-HAA (Victoria, BC) with contributions by: the Laboratoire d'Astrophysique de Marseille (LAM,; Marseille, France) on the development of the convex UV grating; Laboratory for Atmospheric and Space Physics (LASP, University of Colorado) on the development of UV modifications to the TI DMD devices; JPL/Teledyne-e2v/CSA on the delta-doped detectors (§5.3); and the VUVLab (University of Calgary) for the vacuum UV testing (§5.2). The program will develop and test prototypes for each of these components, followed by the assembly of a UVMOS spectrometer test bench that will itself be tested at the VUVLab. This program aims to raise the technology readiness level of the UVMOS instrument to TRL6 by characterizing the use and performance of the integrated system within a vacuum environment and at UV wavelengths.

6 Summary

We have presented a brief overview of the proposed CASTOR mission including its current design, operations model, science program and ongoing development activities. The mission has recently completed a technology risk-reduction study as well as a Phase 0 study, and the team is aiming to move to Phase A in 2025. Since the mission is optimized for high-resolution, wide-field imaging and spectroscopy in the UV/blue-optical region, its scientific capabilities will complement those of JWST, Euclid, Roman and Rubin. Similarly, its sensitivity and angular resolution complement the wide-fields of upcoming UV TDAMM missions (Ultrasat, UVEX). The mission will help bridge a potential gap in UV/optical facilities defined by the end of Hubble operations and the anticipated launch of HWO in the 2040s; indeed, through its planned legacy surveys and GO programs, CASTOR will also help optimize the scientific exploitation of HWO through the selection of the optimal UVOIR targets. Finally, we describe a number of pre-Phase A technology development programs that are now underway, some of which may also be relevant for HWO.

References

1 J. D. Rhodes, R. J. Massey, J. Albert, *et al.*, "The Stability of the Point-Spread Function of the Advanced Camera for Surveys on the Hubble Space Telescope and Implications for Weak Gravitational Lensing," *ApJ Supp.* **172**, 203–218 (2007).

2 Euclid Collaboration, G. Congedo, L. Miller, *et al.*, "Euclid preparation: LIII. LensMC, weak lensing cosmic shear measurement with forward modelling and Markov Chain Monte Carlo sampling," *Astronomy & Astrophysics* **691**, A319 (2024).

3 M. A. Troxel, H. Long, C. M. Hirata, *et al.*, "A synthetic Roman Space Telescope High-Latitude Imaging Survey: simulation suite and the impact of wavefront errors on weak gravitational lensing," *MNRAS* **501**, 2044–2070 (2021).

4 National Academies of Sciences, Engineering, and Medicine, *Pathways to Discovery in Astronomy and Astrophysics for the 2020s* (2021).

5 S. Tuttle, M. Matsumura, D. R. Ardila, *et al.*, "Ultraviolet Technology To Prepare For The Habitable Worlds Observatory," *arXiv e-prints* , arXiv:2408.07242 (2024).

6 P. Côte, A. Scott, M. Balogh, *et al.*, "CASTOR: the Cosmological Advanced Survey Telescope for Optical and Ultraviolet Research," in *Space Telescopes and Instrumentation 2012: Optical, Infrared, and Millimeter Wave*, M. C. Clampin, G. G. Fazio, H. A. MacEwen, *et al.*, Eds., *Society of Photo-Optical Instrumentation Engineers (SPIE) Conference Series* **8442**, 844215 (2012).

7 A. D. Scott, P. Cote, N. Rowlands, *et al.*, "Candidate detector assessment for the CASTOR mission," in *High Energy, Optical, and Infrared Detectors for Astronomy VI*, A. D. Holland and J. Beletic, Eds., *Society of Photo-Optical Instrumentation Engineers (SPIE) Conference Series* **9154**, 91542C (2014).

8 A. Scott, A. Beaton, N. Roy, *et al.*, "NUV performance of e2v large BICMOS array for CASTOR," in *High Energy, Optical, and Infrared Detectors for Astronomy VII*, A. D. Holland and J. Beletic, Eds., *Society of Photo-Optical Instrumentation Engineers (SPIE) Conference Series* **9915**, 99151T (2016).

9 P. Cote, B. Abraham, M. Balogh, *et al.*, "CASTOR: A Flagship Canadian Space Telescope," in *Canadian Long Range Plan for Astronomy and Astrophysics White Papers*, **2020**, 18 (2019).

10 P. Côté, R. Abraham, M. Balogh, *et al.*, "Final Report On the Wide-Field Space Astronomy Study: The Cosmological Advanced Survey Telescope for Optical and UV Research (CASTOR)," *CSA CDRL 7 DID-000* (2019).

11 P. Barmby, B. Gaensler, M. Dobbs, *et al.*, "Discovery at the Cosmic Frontier: Canadian Astronomy Long Range Plan 2020-2030," in *Canadian Long Range Plan for Astronomy and Astrophysics White Papers*, **2020**, 68 (2021).

12 D. C. Martin, J. Fanson, D. Schiminovich, *et al.*, "The galaxy evolution explorer: A space ultraviolet survey mission," *The Astrophysical Journal* **619**, L1 (2005).

13 S. N. Tandon, A. Subramaniam, V. Girish, *et al.*, "In-orbit Calibrations of the Ultraviolet Imaging Telescope," *Astronomical Journal* **154**, 128 (2017).

14 Y. Shvartzvald, E. Waxman, A. Gal-Yam, *et al.*, "ULTRASAT: A Wide-field Time-domain UV Space Telescope," *ApJ* **964**, 74 (2024).

15 S. R. Kulkarni, F. A. Harrison, B. W. Grefenstette, *et al.*, "Science with the ultraviolet explorer (uvex)," (2023).

16 J. J. Dalcanton, B. F. Williams, D. Lang, *et al.*, "The Panchromatic Hubble Andromeda Treasury," *ApJ Supp.* **200**, 18 (2012).

17 I. Cheng, T. E. Woods, P. Côté, *et al.*, "FORECASTOR. I. Finding Optics Requirements and Exposure Times for the Cosmological Advanced Survey Telescope for Optical and UV Research Mission," *Astronomical Journal* **167**, 178 (2024).

18 J. Rhodes, R. C. Nichol, É. Aubourg, *et al.*, "Scientific Synergy between LSST and Euclid," *ApJ Supp.* **233**, 21 (2017).

19 Ž. Ivezić, S. M. Kahn, J. A. Tyson, *et al.*, "LSST: From Science Drivers to Reference Design and Anticipated Data Products," *ApJ* **873**, 111 (2019).

20 M. L. Graham, A. J. Connolly, W. Wang, *et al.*, "Photometric Redshifts with the LSST. II. The Impact of Near-infrared and Near-ultraviolet Photometry," *Astronomical Journal* **159**, 258 (2020).

21 B. R. Scott, A. I. Malz, and R. Sorba, "A holistic exploration of the potentially recoverable redshift information of Stage IV galaxy surveys," *arXiv e-prints*, arXiv:2409.20443 (2024).

22 A. J. Connolly, J. Peterson, J. G. Jernigan, *et al.*, "Simulating the LSST system," in *Modeling, Systems Engineering, and Project Management for Astronomy IV*, G. Z. Angeli and P. Dierickx, Eds., *Society of Photo-Optical Instrumentation Engineers (SPIE) Conference Series* **7738**, 77381O (2010).

23 Ž. Ivezić, S. M. Kahn, J. A. Tyson, *et al.*, "LSST: From Science Drivers to Reference Design and Anticipated Data Products," *ApJ* **873**, 111 (2019).

24 J. Zhang, "The quest for an accurate measurement of cosmic shear," *National Science Review* **3**, 159–160 (2016).

25 Euclid Collaboration, R. Scaramella, J. Amiaux, *et al.*, "Euclid preparation. I. The Euclid Wide Survey," *Astronomy & Astrophysics* **662**, A112 (2022).

26 D. Spergel, N. Gehrels, C. Baltay, *et al.*, "Wide-Field InfrarRed Survey Telescope-Astrophysics Focused Telescope Assets WFIRST-AFTA 2015 Report," *arXiv e-prints* , arXiv:1503.03757 (2015).

27 R. A. Ibata, A. McConnachie, J.-C. Cuillandre, *et al.*, "The Canada-France Imaging Survey: First Results from the u-Band Component," *ApJ* **848**, 128 (2017).

28 C. M. Hirata, M. Yamamoto, K. Laliotis, *et al.*, "Simulating image coaddition with the Nancy Grace Roman Space Telescope - I. Simulation methodology and general results," *MNRAS* **528**, 2533–2561 (2024).

29 Y. Gong, X. Liu, Y. Cao, *et al.*, "Cosmology from the Chinese Space Station Optical Survey (CSS-OS)," *ApJ* **883**, 203 (2019).

30 J. E. Schlieder, T. Barclay, A. Barnes, *et al.*, "Survey science with the Nancy Grace Roman Space Telescope Wide Field Instrument," in *Space Telescopes and Instrumentation 2024: Optical, Infrared, and Millimeter Wave*, L. E. Coyle, S. Matsuura, and M. D. Perrin, Eds., *Society of Photo-Optical Instrumentation Engineers (SPIE) Conference Series* **13092**, 130920S (2024).

31 P. E. Dewdney, P. J. Hall, R. T. Schilizzi, *et al.*, "The Square Kilometre Array," *IEEE Proceedings* **97**, 1482–1496 (2009).

32 P. S. Cowperthwaite, E. Berger, V. A. Villar, *et al.*, "The Electromagnetic Counterpart of the Binary Neutron Star Merger LIGO/Virgo GW170817. II. UV, Optical, and Near-infrared Light Curves and Comparison to Kilonova Models," *ApJL* **848**, L17 (2017).

33 V. Korol, N. Hallakoun, S. Toonen, *et al.*, "Observationally driven Galactic double white dwarf population for LISA," *MNRAS* **511**, 5936–5947 (2022).

34 R. I. Hynes, C. A. Haswell, W. Cui, *et al.*, "The remarkable rapid X-ray, ultraviolet, optical and infrared variability in the black hole XTE J1118+480," *MNRAS* **345**, 292–310 (2003).

35 P. Gandhi, V. S. Dhillon, M. Durant, *et al.*, "Rapid optical and X-ray timing observations of GX339-4: multicomponent optical variability in the low/hard state," *MNRAS* **407**, 2166–2192 (2010).

36 E. M. Cackett, M. C. Bentz, and E. Kara, "Reverberation mapping of active galactic nuclei: from X-ray corona to dusty torus," *iScience* **24**, 102557 (2021).

37 R. Takahashi, "Arrival Time Differences between Gravitational Waves and Electromagnetic Signals due to Gravitational Lensing," *ApJ* **835**, 103 (2017).

38 R. Antonucci, "Unified models for active galactic nuclei and quasars.," *ARA & A* **31**, 473–521 (1993).

39 A. C. Fabian, "Observational Evidence of Active Galactic Nuclei Feedback," *ARA & A* **50**, 455–489 (2012).

40 B. M. Peterson, L. Ferrarese, K. M. Gilbert, *et al.*, "Central Masses and Broad-Line Region Sizes of Active Galactic Nuclei. II. A Homogeneous Analysis of a Large Reverberation-Mapping Database," *ApJ* **613**, 682–699 (2004).

41 A. Kolodzig, M. Gilfanov, R. Sunyaev, *et al.*, "AGN and QSOs in the eROSITA All-Sky Survey. I. Statistical properties," *Astronomy & Astrophysics* **558**, A89 (2013).

42 A. C. Fabian, "Observational Evidence of Active Galactic Nuclei Feedback," *ARA & A* **50**, 455–489 (2012).

43 S. Kaspi, P. S. Smith, H. Netzer, *et al.*, "Reverberation Measurements for 17 Quasars and the Size-Mass-Luminosity Relations in Active Galactic Nuclei," *ApJ* **533**, 631–649 (2000).

44 C. L. MacLeod, N. P. Ross, A. Lawrence, *et al.*, "A systematic search for changing-look quasars in SDSS," *MNRAS* **457**, 389–404 (2016).

45 P. Cote, B. Abraham, M. Balogh, *et al.*, "CASTOR: A Flagship Canadian Space Telescope," in *Canadian Long Range Plan for Astronomy and Astrophysics White Papers*, **2020**, 18 (2019).

46 T. E. Woods, R. Alexandroff, S. Ellison, *et al.*, "Revealing the Origin and Cosmic Evolution of Supermassive Black Holes," in *Canadian Long Range Plan for Astronomy and Astrophysics White Papers*, **2020**, 34 (2019).

47 The MSE Science Team, C. Babusiaux, M. Bergemann, *et al.*, "The Detailed Science Case for the Maunakea Spectroscopic Explorer, 2019 edition," *arXiv e-prints* , arXiv:1904.04907 (2019).

48 N. Tamura, N. Takato, A. Shimono, *et al.*, "Prime Focus Spectrograph (PFS) for the Subaru telescope: overview, recent progress, and future perspectives," in *Ground-based and Airborne Instrumentation for Astronomy VI*, C. J. Evans, L. Simard, and H. Takami, Eds., *Society of Photo-Optical Instrumentation Engineers (SPIE) Conference Series* **9908**, 99081M (2016).

49 R. Bacon, V. Maineiri, S. Randich, *et al.*, "WST - Widefield Spectroscopic Telescope: motivation, science drivers and top level requirements for a new dedicated facility," in *Ground-based and Airborne Telescopes X*, H. K. Marshall, J. Spyromilio, and T. Usuda, Eds., *Society of Photo-Optical Instrumentation Engineers (SPIE) Conference Series* **13094**, 130941O (2024).

50 D. Zhang, "A Review of the Theory of Galactic Winds Driven by Stellar Feedback," *Galaxies* **6**, 114 (2018).

51 P. Madau and M. Dickinson, "Cosmic Star-Formation History," *ARA & A* **52**, 415–486 (2014).

52 J. S. Vink, "Star Formation in the Ultraviolet," *Galaxies* **8**, 43 (2020).

53 M. A. Marshall, L. Amen, T. E. Woods, *et al.*, "FORECASTOR – II. Simulating Galaxy Surveys with the Cosmological Advanced Survey Telescope for Optical and UV Research," *arXiv e-prints* , arXiv:2402.17163 (2024).

54 Gaia Collaboration, A. Vallenari, A. G. A. Brown, *et al.*, "Gaia Data Release 3. Summary of the content and survey properties," *Astronomy & Astrophysics* **674**, A1 (2023).

55 A. Helmi, "The stellar halo of the Galaxy," *Astronomy & Astrophysics Review* **15**, 145–188 (2008).

56 T. Eifler, H. Miyatake, E. Krause, *et al.*, "Cosmology with the Roman Space Telescope - multiprobe strategies," *MNRAS* **507**, 1746–1761 (2021).

57 A. McConnachie, M. Balogh, J. Bovy, *et al.*, "The next decade of optical wide field astronomy in Canada," in *Canadian Long Range Plan for Astronomy and Astrophysics White Papers*, **2020**, 25 (2019).

58 S. Sharma, J. Bland-Hawthorn, K. V. Johnston, *et al.*, "Galaxia: A code to generate a synthetic survey of the milky way," *The Astrophysical Journal* **730**(1), 3 (2011).

59 R. Gratton, A. Bragaglia, E. Carretta, *et al.*, "What is a globular cluster? An observational perspective," *Astronomy & Astrophysics Review* **27**, 8 (2019).

60 G. F. Thomas, J. Jensen, A. McConnachie, *et al.*, "The Hidden Past of M92: Detection and Characterization of a Newly Formed 17° Long Stellar Stream Using the Canada-France Imaging Survey," *ApJ* **902**, 89 (2020).

61 A. Frebel and J. E. Norris, "Near-Field Cosmology with Extremely Metal-Poor Stars," *ARA & A* **53**, 631–688 (2015).

62 J. L. Linsky, "UV astronomy throughout the ages: a historical perspective," *Astrophysics and Space Science* **363**, 101 (2018).

63 B. E. Westerlund, "The Magellanic Clouds: their evolution, structure and composition," *Astronomy & Astrophysics Review* **2**, 29–78 (1990).

64 R. L. Gilliland, T. M. Brown, P. Guhathakurta, *et al.*, "A Lack of Planets in 47 Tucanae from a Hubble Space Telescope Search," *ApJL* **545**, L47–L51 (2000).

65 D. T. F. Weldrake, P. D. Sackett, T. J. Bridges, *et al.*, "An Absence of Hot Jupiter Planets in 47 Tucanae: Results of a Wide-Field Transit Search," *ApJ* **620**, 1043–1051 (2005).

66 B. Zuckerman, C. Melis, B. Klein, *et al.*, "Ancient Planetary Systems are Orbiting a Large Fraction of White Dwarf Stars," *ApJ* **722**, 725–736 (2010).

67 A. Vanderburg, J. A. Johnson, S. Rappaport, *et al.*, "A disintegrating minor planet transiting a white dwarf," *Nature* **526**, 546–549 (2015).

68 M. E. Brown, "The compositions of kuiper belt objects," *Annual Review of Earth and Planetary Sciences* **40**(Volume 40, 2012), 467–494 (2012).

69 R. Malhotra, "Resonant Kuiper belt objects: a review," *Geoscience Letters* **6**, 12 (2019).

70 M. Duncan, T. Quinn, and S. Tremaine, "The Formation and Extent of the Solar System Comet Cloud," *Astronomical Journal* **94**, 1330 (1987).

71 S. Portegies Zwart, "Oort cloud Ecology. I. Extra-solar Oort clouds and the origin of asteroidal interlopers," *Astronomy & Astrophysics* **647**, A136 (2021).

72 M. T. Bannister, B. J. Gladman, J. J. Kavelaars, *et al.*, "Ossos. vii. 800+ trans-neptunian objects—the complete data release," *The Astrophysical Journal Supplement Series* **236**, 18 (2018).

73 S. Gaudet, N. Hill, P. Armstrong, *et al.*, "CANFAR: the Canadian Advanced Network for Astronomical Research," in *Software and Cyberinfrastructure for Astronomy*, N. M. Radziwill and A. Bridger, Eds., *Society of Photo-Optical Instrumentation Engineers (SPIE) Conference Series* **7740**, 77401I (2010).

74 S. Fabbro, B. Major, D. Jenkins, *et al.*, "Innovations and impact of the CANFAR science platform," in *Society of Photo-Optical Instrumentation Engineers (SPIE) Conference Series*, J. Ibsen and G. Chiozzi, Eds., *Society of Photo-Optical Instrumentation Engineers (SPIE) Conference Series* **13101**, 131011I (2024).

75 J. F. Rowe, S. Metchev, K. L. Hoffman, *et al.*, "The POET mission: a Canadian space telescope for exoplanet astrophysics," in *Space Telescopes and Instrumentation 2022: Optical, Infrared, and Millimeter Wave*, L. E. Coyle, S. Matsuura, and M. D. Perrin, Eds., *Society of Photo-Optical Instrumentation Engineers (SPIE) Conference Series* **12180**, 121800A (2022).

76 J. Glover, I. Cheng, T. E. Woods, *et al.*, "FORECASTOR: an exposure time calculator for the CASTOR space mission simulating UVMOS spectroscopy," in *Society of Photo-Optical Instrumentation Engineers (SPIE) Conference Series*, J.-W. A. den Herder, S. Nikzad, and K. Nakazawa, Eds., *Society of Photo-Optical Instrumentation Engineers (SPIE) Conference Series* **12181**, 1218177 (2022).

77 L. Y. A. Yung, R. S. Somerville, H. C. Ferguson, *et al.*, "Semi-analytic forecasts for JWST - VI. Simulated light-cones and galaxy clustering predictions," *MNRAS* **515**, 5416–5436 (2022).

78 L. Y. A. Yung, R. S. Somerville, S. L. Finkelstein, *et al.*, "Semi-analytic forecasts for Roman - the beginning of a new era of deep-wide galaxy surveys," *MNRAS* **519**, 1578–1600 (2023).

79 B. T. P. Rowe, M. Jarvis, R. Mandelbaum, *et al.*, "GALSIM: The modular galaxy image simulation toolkit," *Astronomy and Computing* **10**, 121–150 (2015).

80 J. P. Greco and S. Danieli, "ArtPop: A Stellar Population and Image Simulation Python Package," *ApJ* **941**, 26 (2022).

81 M. Arko, T. Prod'homme, F. Lemmel, *et al.*, "Pyxel 1.0: an open source Python framework for detector and end-to-end instrument simulation," *Journal of Astronomical Telescopes, Instruments, and Systems* **8**, 048002 (2022).

82 J. Postma, J. B. Hutchings, and D. Leahy, "Calibration and Performance of the Photon-counting Detectors for the Ultraviolet Imaging Telescope (UVIT) of the Astrosat Observatory," *Publications of the Astronomical Society of the Pacific* **123**, 833 (2011).

83 D. Leahy, J. Postma, J. B. Hutchings, *et al.*, "The Calibration of the UVIT Detectors for the ASTROSAT Observatory," in *IAU General Assembly*, 487–491 (2020).

84 M. E. Hoenk, P. J. Grunthaner, F. J. Grunthaner, *et al.*, "Growth of a delta-doped silicon layer by molecular beam epitaxy on a charge-coupled device for reflection-limited ultraviolet quantum efficiency," *Applied Physics Letters* **61**, 1084–1086 (1992).

85 S. Nikzad, A. D. Jewell, M. E. Hoenk, *et al.*, "High-efficiency UV/optical/NIR detectors for large aperture telescopes and UV explorer missions: development of and field observations with delta-doped arrays," *Journal of Astronomical Telescopes, Instruments, and Systems* **3**, 036002 (2017).

86 J. Skottfelt, C. Crews, B. Dryer, *et al.*, "Evaluating UV detector enhancement technologies for the next generation of space telescopes: the path to CASTOR," in *Space Telescopes and Instrumentation 2024: Ultraviolet to Gamma Ray*, J.-W. A. den Herder, S. Nikzad, and K. Nakazawa, Eds., **13093**, 130933W, International Society for Optics and Photonics, SPIE (2024).

87 F. Zamkotsian, P. Spano, P. Lanzoni, *et al.*, "BATMAN: a DMD-based multi-object spectrograph on Galileo telescope," in *Ground-based and Airborne Instrumentation for Astronomy V*, S. K. Ramsay, I. S. McLean, and H. Takami, Eds., *Society of Photo-Optical Instrumentation Engineers (SPIE) Conference Series* **9147**, 914713 (2014).

88 F. Zamkotsian, P. Lanzoni, N. Tchoubaklian, *et al.*, "BATMAN @ TNG: instrument integration and performance," in *Ground-based and Airborne Instrumentation for Astronomy VII*, C. J. Evans, L. Simard, and H. Takami, Eds., *Society of Photo-Optical Instrumentation Engineers (SPIE) Conference Series* **10702**, 107025P (2018).

89 A. Kutyrev, M. Greenhouse, M.-P. Chang, *et al.*, "Scalable microshutter focal plane masks for UV, visible, and infrared spectroscopy," in *UV, X-Ray, and Gamma-Ray Space Instrumentation for Astronomy XXIII*, O. H. Siegmund and K. Hoadley, Eds., **12678**, 126780Q, International Society for Optics and Photonics, SPIE (2023).

90 K. Kim, M.-P. Chang, A. S. Kutyrev, *et al.*, "Technological developments of NexGen Micro-Shutter Array (NGMSA) for the future Habitable Worlds Observatory (HWO) flagship mission," in *Advances in Optical and Mechanical Technologies for Telescopes and Instrumentation VI*, R. Navarro and R. Jedamzik, Eds., **13100**, 131001N, International Society for Optics and Photonics, SPIE (2024).

91 A. Travinsky, D. Vorobiev, Z. Ninkov, *et al.*, "Evaluation of digital micromirror devices for use in space-based multiobject spectrometer application," *Journal of Astronomical Telescopes, Instruments, and Systems* **3**, 035003 (2017).

92 D. Vorobiev, J. Del Hoyo, M. Quijada, *et al.*, "Development of digital micromirror devices (DMDs) for far-UV applications," in *Advances in Optical and Mechanical Technologies for Telescopes and Instrumentation III*, R. Navarro and R. Geyl, Eds., *Society of Photo-Optical Instrumentation Engineers (SPIE) Conference Series* **10706**, 107062F (2018).

93 F. Zamkotsian, R. Krähenbühl, P. Lanzoni, *et al.*, "Convex blazed gratings for high throughput spectrographs in space missions," in *Society of Photo-Optical Instrumentation Engineers (SPIE) Conference Series*, K. Minoglou, N. Karafolas, and B. Cugny, Eds., *Society of Photo-Optical Instrumentation Engineers (SPIE) Conference Series* **12777**, 127772J (2023).

List of Figures

2   Total system throughput, η, versus wavelength for several high-resolution space telescopes. CASTOR will complement red-optical/IR imaging from JWST, Euclid and Roman. Its wide-field imager uses dichroics to provide simultaneous three-band imaging over the 0.15 to 0.55 μm wavelength range. A deployable broadband filter allows users to subdivide the UV and u channels (dashed curves).

3   (Left) Illustration of the main payload elements for the telescope (see §2.1, §2.2 and §2.5 for details). (Right) Schematic diagram showing the opto-mechanical design of the telescope. An off-axis, three-mirror anastigmat design uses a fine steering mirror for image stabilization and two dichroics to direct the incoming light onto three focal plane arrays (FPAs).

4   Zerodur fine steering mirror (FSM) prototype, without reflective coating, undergoing wavefront error testing at the ABB Measurement and Analytics facility in Quebec City. The fully functional FSM tip-tilt mechanism is mounted on a damped optical table, in front of a Zygo interferometer. See §2.3 for details.

5   A schematic view of CASTOR's instrument suite. Simultaneous wide-field imaging in the UV, u and g passbands is enabled by dichroics that divide the incoming light into three channels covering the 0.15 to 0.55 μm range. A deployable grism provides low-resolution ($300 \lesssim R \lesssim 420$) slit-less spectroscopy over the full imaging field, in the UV and u channels. Each of CASTOR's three focal plane arrays (FPAs) is accompanied by a dedicated CMOS detector for high-precision photometric measurements of transiting exoplanets. Medium resolution long-slit and multi-slit spectroscopy is possible using a UVMOS instrument that observes an adjacent field. Two CMOS devices in the $g-$band channel provide spacecraft guiding.

6   Point spread functions (PSFs) at the field center in each of CASTOR's UV, u and g channels (left to right, respectively).[17]

7   CASTOR will be mounted on the MAC-200 satellite bus from Magellan Aerospace Corporation. This bus is pictured during assembly of the Radarsat Constellation Mission which launched in 2019. For more details, see §2.5.

8   (Left) Preliminary division of observing time recommended in the Phase 0 study; see §3 for details. (Right) Division of observing time by instrument for the 14 candidate legacy surveys from the Phase 0 study and summarized in Table 3. Surveys will be refined in subsequent phases according to developments in the international astronomy landscape and partner requirements.

9   (Left) Depths of wide-field UV/optical/IR imaging surveys plotted as a function of wavelength. Results are shown for several survey: UNIONS,[27] LSST,[19] Euclid-Wide,[25] Roman-HLWA,[28] CSS-OS[29] and CASTOR Wide. Note that CASTOR Wide targets the same footprint as the Roman HLWA survey. The labels under each filter indicate the survey's approximate image quality (i.e., EE50 radius). (Right) Predicted improvements in the determination of SFR (upper panels) and specific SFR (lower panels) from the CASTOR Wide Survey (right panels) compared to the GALEX Medium-Deep Survey (left panels). The gains are most dramatic for quenching galaxies located in the transitional zone (i.e., the Green Valley).

10   Mock CASTOR observations of a GW170817-like kilonovae at 150 Mpc using our baseline survey strategy described below. (Left). Expected observations for a transient with both a red (heavy r-process elements) and a blue (light r-process elements) ejecta component. (Right). Expected observations for a transient with only a red ejecta component. While the infrared emission (yellow curve) is almost unchanged, dramatic differences are evident in the ultraviolet and blue bands on a timescale of 1-10 days. Even at these moderate distances, tracing the evolution of the UV emission requires depths of $> 25 - 26$ mag AB. Quoted depths of various proposed UV/$u-$band survey missions are highlighted (with depth indicated at the upper boundary of each shaded region).

11   Luminosity-redshift parameter space spanned by CASTOR (light gray area) compared to all previous studies (colored symbols). CASTOR will be able to probe uniformly a unique region in the phase space of redshift and luminosity (black circles showing a simulated sample in 5 deg^2) as well as galaxy-host properties to study how black holes grow and how they affect galaxy evolution over 10 billion years of cosmic time.

12   A simulation of part of the Hubble Ultra Deep Field (UDF) in passbands from CASTOR (u, g) and Roman (F184). This image shows a $\sim 1\rlap{.}'5 \times 1\rlap{.}'5$ field, or just $\sim 0.06\%$ of the area that will be covered by the proposed Ultra-Deep Survey. While Roman's IR imaging (red) is sensitive to existing stellar mass, CASTOR picks out regions of ongoing star formation. With comparable spatial resolution from the UV to the near-IR it will be possible to map stellar populations and other physical parameters across galaxies, out to cosmic noon.

13   Mock CASTOR observations of the Pal 5 stellar stream (at a distance of 20 kpc) based on an N-body simulation of the stream (orange points in top panel) inside a smooth Milky Way halo (D. Erkal, private communication) combined with background/foreground contamination from Galaxia[58] stellar catalogues in fields surrounding the stream (blue points). On-sky positions of the stars are shown in the top and right panels. Panel C shows a selection based on the CASTOR proper motions (from panel B). A further selection based on the CASTOR colour-magnitude diagram (from panel D; along the metal-poor isochrone corresponding to the stream) is shown in panel E, where the stream appears as a clear overdensity. CASTOR's deeper observations (compared to Gaia) with a proper motion precision corresponding to 50 km/s or better at this distance (fainter stars with poorer proper motion precision are not included in this figure) will significantly increase the number of stream members identified, improve the contrast, and reveal an unprecedented view of stellar streams and their morphology.

14   Observations of a $100'' \times 100''$ region in 30 Doradus from GALEX/NUV (left) and simulated CASTOR observations (right) based on smoothed data from HST/WFC3 F275W. The depth is 24 mag, so the CASTOR Magellanic Clouds survey will reach about 50 times deeper.

15   Simulations of the TNO wide survey component from a high precision model of the outer Solar System.[72] The wide footprint will include all objects within 6° of the ecliptic and having $\delta < 0°$, the region that will be best sampled by LSST. Colored points show the objects detected by the wide component of the CASTOR census of TNOs. Red symbols show objects are detected in both u and g; blue symbols show objects detected in g only. For clarity, the figure shows only 10% of total model and detected objects and only the 12h-24h zone, the part of the ecliptic south of the equatorial plane.

16   Point-source sensitivity (AB mag) in each of CASTOR's three primary passbands, expressed as the time needed to reach a signal-to-noise ratio of S/N = 5. The time for CASTOR to complete a single orbit is shown as the dashed horizontal line.

17   Sample screenshot from the web application developed for the FORECASTOR suite on the CANFAR Science Platform.[17]

18   Simulated CASTOR grism spectrum of a Lyman-break galaxy at $z = 2.793$. The top left panel shows the simulated direct image of the source ($r_{\mathrm{eff}} = 0.15''$, ellipticity of 0.55, Sérsic index $n = 1.05$) at CASTOR resolution. The top right panel shows the Lyman-break template used for the source SED. The shaded bands show the wavelength range of the CASTOR UV, u, and g channels (purple, cyan, and hatched green, respectively). Only the UV and u channels have grism capabilities. The bottom panel shows the noiseless electron counts of the simulated grism spectrum after 6 hr of exposure for a $u = 23.4$ mag (AB) source. The grism tool also simulates the noise properties of the grism observations (including the sky background, read noise and dark current) to produce SNR maps and derive exposure times.

19   Simulated images for a small patch of CASTOR's planned Wide Survey in the UV, u, and g channels, generated using a synthetic light-cone catalog drawn from published semi-analytic models of galaxy populations.[77,78] With total exposure times in the range 1000–2000 sec, these images reach 5σ point-source depths of $\sim$ 27.5 in all three channels.

20   (*Left*) View of the exterior hardware. (*Right*) Manipulator mounted inside of the vacuum vessel.

21   Two views of the CIS120 detector and platen installed in the cryostat at NRC-HAA.

22   CIS120 and monochromator test setup at The Open University. A CIS120 device is mounted inside the vacuum chamber on the left, currently set up for dark tests. The chamber on the right is a housing for a dual deuterium and halogen lamp feeding the monochromator in the middle.

23   Front and side view of the UVMOS optomechanical concept. OM1 and OM2 refer to the first and second Offner mirrors.

List of Tables